NASA TECHNICAL NOTE

NASA TN D-4900

NASA TN D-4900
C.1



# ANALYSIS OF NUMERICAL INTEGRATION TECHNIQUES FOR REAL-TIME DIGITAL FLIGHT SIMULATION

*by John W. Wilson and George G. Steinmetz*

*Langley Research Center*
*Langley Station, Hampton, Va.*

NATIONAL AERONAUTICS AND SPACE ADMINISTRATION • WASHINGTON, D. C. • NOVEMBER 1968

NASA TN D-4900

# ANALYSIS OF NUMERICAL INTEGRATION TECHNIQUES FOR REAL-TIME DIGITAL FLIGHT SIMULATION

By John W. Wilson and George G. Steinmetz

Langley Research Center
Langley Station, Hampton, Va.

NATIONAL AERONAUTICS AND SPACE ADMINISTRATION

For sale by the Clearinghouse for Federal Scientific and Technical Information
Springfield, Virginia 22151 – CFSTI price $3.00

CONTENTS


| | Page |
|---|---|
| SUMMARY | 1 |
| INTRODUCTION | 1 |
| SYMBOLS | 3 |
| PROBLEM DESCRIPTION | 11 |
| Background Discussion | 11 |
| Fundamental Differential Equations | 11 |
| ANALYSIS | 14 |
| Roundoff and Truncation | 15 |
| Axis Transformations | 22 |
| Attitude Control System | 31 |
| Moment Equations | 35 |
| Translational Dynamics | 47 |
| TWO EXAMPLE PROBLEMS | 48 |
| Gemini-Agena Problem | 48 |
| Gemini-Agena Tether Problem | 50 |
| RESULTS AND DISCUSSION | 53 |
| APPLICATIONS | 54 |
| CONCLUDING REMARKS | 56 |
| APPENDIX A – GEMINI-AGENA EQUATIONS OF MOTION | 59 |
| Equations of Motion | 59 |
| Simulation Hardware Equations | 66 |
| Cockpit Instrument and Auxiliary Equations | 68 |
| APPENDIX B – DERIVATION OF GREEN'S FUNCTION TECHNIQUE | 70 |
| REFERENCES | 79 |
| TABLES | 81 |
| FIGURES | 83 |

# ANALYSIS OF NUMERICAL INTEGRATION TECHNIQUES FOR REAL-TIME DIGITAL FLIGHT SIMULATION

By John W. Wilson and George G. Steinmetz

Langley Research Center

## SUMMARY

Low-order numerical integration techniques are analyzed and established as adequate for digital simulation of man-in-the-loop nonaerodynamic rigid-body problems. In addition to low-order integration techniques, a Green's function approach is presented for the solution of the gyroscope equations. This approach yields an exact solution to the gyroscope output for the simulated forcing function with virtually no limitation on the integration interval size. Effects of roundoff error are shown to be marginal for the translational dynamics with solution rates on the order of 32 solutions per second on a floating-point machine with a 27-bit fractional part.

Two example problems were solved by using the techniques established. A Gemini-Agena eleven-degree-of-freedom problem was programed in FORTRAN and then modified to a Gemini-Agena elastically coupled system. Primary concern was given to minimizing the time required of the arithmetic unit. The results of these problems indicate the utility of the IBM 7094 class of computers for this type of problem since only a small fraction of the memory and arithmetic processing time was used (10 to 15 percent each). This study strongly supports the desirability of multiprograming to alleviate inefficiency on a more sophisticated machine.

## INTRODUCTION

In the past few years, general-purpose digital computers have played an important role in meeting resolution and accuracy requirements of real-time simulation problems. (See ref. 1, p. R34.) However, the extensive use of digital computing equipment has been prohibited (ref. 1, pp. R29-R30) except in special applications. (See ref. 2.) In the early years of the 1960 decade, general-purpose digital computers of sufficient speed and storage were available at a cost that was competitive (at least for the larger simulation problems; ref. 1, p. R31, fig. 3) with general-purpose analog equipment. Even so, the general-purpose analog facility, which is a composite of several basic computers, could be tied together in different combinations to perform one large simulation or several

smaller simulations; this arrangement provides an efficiency advantage that the general-purpose digital computer did not yet enjoy. The capacity of the digital computer was determined by the largest problem to be solved and was totally dedicated to the solution of a smaller problem; thus, a large amount of idle central processor time and core remained unused. This fact led many simulation laboratories to develop software capable of doing more than one simulation on a "one computer complex either simultaneously or alternatively." (See ref. 3, p. 249.) The methods used required concurrent compilation (multiprocessing) of both problems (ref. 3, p. 250). The next logical step in software development, which is a necessity for a general-purpose simulation laboratory, is the ability to process and/or compile more than one problem independently (multiprograming) on one general-purpose computer.

With the advent of the next generation of digital computers, one envisions the utility of multiprograming in an effort to reduce cost in a general-purpose simulation laboratory. The removal of the restriction that the computer be dedicated to a fixed number of problems imposes greater demands on the simulation programer. It is no longer sufficient merely to generate a working program, but it now becomes imperative that the most efficient way to mechanize a given simulation problem be determined.

In transforming a simulation problem to a digital program, attention must be given to algorithms to approximate required mathematical functions. The analysis and development of integration algorithms or integration schemes shall be the body of this report. In recent years, there has been a general transfer of large simulation problems either whole or in part to digital computing equipment. As is true in any new field, the points of view usually cover a wide spectrum and the use of integration schemes in real-time simulation is no exception as witnessed in references 1, 2, and 4 to 9.

The general problem of differential-equation solving has led to many varied types of integration techniques which are usually complicated and often time consuming, the attempt usually being made to solve the widest possible class of problems most of the time. However, these techniques are often too slow and complicated for effective use in real-time problems. The approach taken in this paper is to consider only a rather restricted class of differential equations from a real-time point of view. The hope is to produce a fresh look at real-time simulation that is on a sound analytical and experimental basis.

Consideration is given in this report to the simulation of nonaerodynamic rigid vehicles with on-off control. The results however will in part be applicable to most flight-vehicle simulations. The accuracy requirement is to meet or exceed that of a corresponding analog solution (usually quoted on the order of 1 percent but not always acquired). The purpose of this report is to establish guidelines for meeting accuracy

requirements of this class of real-time simulation problems and to maintain a high degree of computer efficiency.

The basic equations used to simulate the Gemini-Agena configuration are given in an appendix by Roland L. Bowles of the Langley Research Center.

## SYMBOLS

The International System of Units (SI) are employed in this report. For conversion to U.S. Customary Units, consult reference 10. All systems used throughout this paper are right-hand, orthogonal, Cartesian coordinate systems. (See fig. 1.)

| | |
|---|---|
| A | transformation matrix relating observer (Gemini) body axes and target (Agena) local vertical axes, dimensionless |
| $\bar{A}$ | column vector with components a, b, c, and d, dimensionless |
| a,b,c,d | quaternion elements (Euler parameters), dimensionless |
| $a_{ij}$ | matrix elements of A (i,j = 1,2,3), dimensionless |
| B | transformation matrix relating observer vehicle body axes to inertial frame, dimensionless |
| B' | transformation matrix relating target vehicle body axes to inertial frame, dimensionless |
| $b_{ij}$ | matrix elements of B, dimensionless |
| $b_{ij}'$ | matrix elements of B', dimensionless |
| D | matrix relating the target vehicle axes to a line-of-sight axis system, dimensionless |
| $d_{ij}$ | matrix elements of D, dimensionless |
| E | enlargement or displacement operator, dimensionless |
| e,f,g,h | target quaternion elements, dimensionless |

$F$ matrix relating observer vehicle axes to target vehicle axes, dimensionless

$F_o$ total initial fuel, kilograms

$F_{trans}, F_{att}$ percent fuel used by translational and attitude control systems, respectively, percent

$f_{ij}$ elements of the matrix $F$, dimensionless

$G(t)$ Green's function of linear gyroscope, dimensionless

$G^{\dagger}(t)$ associated Green's function of linear gyroscope, dimensionless

$g_e$ acceleration at surface of earth due to gravitational attraction, 9.84 meters/second$^2$

$g_o$ gravity acceleration at $r_s = r_o$, meters/second$^2$

$\bar{H}$ target vehicle rotational angular momentum vector, kilograms-meter$^2$/second

$H_1, H_2, H_3$ components of target angular momentum vector $\bar{H}$ resolved into target body axes, kilogram-meter$^2$/second

$h$ integration interval size, seconds

$I$ inertial matrix of observer vehicle, kilogram-meter$^2$

$I^{-1}$ inverse of observer vehicle's inertia matrix, (kilogram-meter$^2$)$^{-1}$

$I_{ij}$ elements of matrix $I$, kilogram-meter$^2$

$I_{ij}'$ elements of matrix $I^{-1}$, (kilogram-meter$^2$)$^{-1}$

$I_{sp}$ specific impulse of observer-vehicle reaction control system, second

$i$ imaginary unit, $\sqrt{-1}$

$J$ inertia matrix of target vehicle, kilogram-meter$^2$

$J^{-1}$ inverse of target vehicle's inertia matrix, (kilogram-meter$^2$)$^{-1}$

$J_{ij}$ elements of the matrix J, kilogram-meter$^2$

$J_{ij}'$ elements of the matrix $J^{-1}$, (kilogram-meter$^2$)$^{-1}$

$K_i$ thrust misalinements (i = 1,2,. . .,5), dimensionless

$K_o + 1$ normalized target orbital angular momentum per unit mass, dimensionless

$K_\epsilon$ gain constant used in maintaining orthogonality of transformation matrix

$\bar{L}$ observer vehicle rotational angular momentum vector, kilogram-meter$^2$/second

$L_1, L_2, L_3$ components of observer-vehicle rotational angular momentum $\bar{L}$ resolved into observer body axes, kilogram-meter$^2$/second

$\bar{l}$ column vector of partitioned direction cosine matrix, dimensionless

$l$,m,n partitioned components of direction cosine rate equations (components of $\bar{l}$), dimensionless

$\bar{M}$ moment vector acting on observer vehicle due to translational and attitude control reaction jets, joules

$M_1, M_2, M_3$ components of vector $\bar{M}$, joules

$(M_i)_{T_{\phi\pm}}, (M_i)_{T_{\theta\pm}}, (M_i)_{T_{\psi\pm}}$ X-components of attitude control moments, joules

$(M_i)_{T_{X\pm}}, (M_i)_{T_{Y\pm}}, (M_i)_{T_{Z\pm}}$ X-components of moment resulting from translational control forces, joules

$(M_2)_{T_{\theta\pm}}$ Y-components of attitude control moments, joules

$(M_2)_{T_{X\pm}}, (M_2)_{T_{Y\pm}}, (M_2)_{T_{Z\pm}}$ Y-components of moment resulting from translational control forces, joules

$(M_3)_{T_{\psi\pm}}$ Z-components of attitude control moments, joules

$(M_3)_{T_{X\pm}}, (M_3)_{T_{Y\pm}}, (M_3)_{T_{Z\pm}}$ Z-components of moment resulting from translational control forces, joules

$m$ mass of observer vehicle, kilograms

$\Delta m_{att}, \Delta m_{tran}$ mass changes resulting from translational and attitude reaction control jets, respectively, kilograms

$N$ total rotational angular momentum of observer vehicle squared, $(\text{kilogram-meter}^2/\text{second})^2$

$N_b$ number of significant binary bits, dimensionless

$n,N$ integers, dimensionless

$O(h^n)$ remainder in a series with lowest order term of $h^n$

$P$ norm squared of $\bar{A}$, dimensionless

$p,q,r$ components of observer angular velocity vector $\bar{\omega}$ resolved into observer vehicle axes, radians/second

$p_t,q_t,r_t$ components of target angular velocity vector $\bar{\omega}_t$ resolved into target vehicle axes, radians/second

$p_g,q_g,r_g$ angular velocity components $p$, $q$, $r$ measured by gyroscopes, radians/second

$Q$ norm squared of $\bar{l}$, dimensionless

$\bar{R}$ relative range vector directed from center of gravity of target vehicle to center of gravity of observer vehicle, meters

$\dot{R}$ relative range rate, meters/second

$\bar{R}_{los}$ line-of-sight range vector, meters

$R_{X,o}, R_{Y,o}, R_{Z,o}$ components of relative range vector $\bar{R}$ resolved in observer vehicle axes, meters

$r_e$ mean radius of earth, meters

$r_o$ radius of target reference orbit, meters

$\bar{r}_s$ position vector of target vehicle in a coordinate system with origin at earth's center and coordinate directions always parallel to an inertial frame, meters

$r_s, \theta_s$ polar coordinates locating the center of gravity of target vehicle with respect to inertial space (for elliptic orbits $\theta_s = \pi/2$ at perigee), meters and radians, respectively

S skew-symmetric matrix that relates time rate of change of components of a constant magnitude quaternion to its components referenced to a rotating frame, radians/second

s Laplace transform variable

$T_X, T_Y, T_Z$ components of observer vehicle thrust forces resolved in target local vertical axes, newtons

$T_{X\pm}, T_{Y\pm}, T_{Z\pm}$
$T_{\phi\pm}, T_{\theta\pm}, T_{\psi\pm}$ magnitudes of on-off reaction control jets, newtons

$T_{X,b}, T_{Y,b}, T_{Z,b}$ total forces along observer vehicle axes resulting from translation and attitude control jets, newtons

t time, seconds

V target tangential velocity component ($V = r_s \dot{\theta}_s$), meters/second

$V_o$ characteristic velocity of a vehicle in a circular orbit at radial distance $r_o$, meters/second

$\Delta V$ total velocity change using translational control, meters/second

$\Delta V_X, \Delta V_Y, \Delta V_Z$ components of velocity change using translational control along observer's X, Y, and Z axes, respectively, meters/second

X,Y,Z components of relative range vector $\bar{R}$ referenced to a rotating coordinate frame with origin located at center of gravity of target vehicle, meters

$X_p, Y_p, Z_p$ coordinates of pilot's eye with respect to observer vehicle axes, meters

$\Delta X, \Delta Y, \Delta Z$ components of $\bar{R}_{los}$ resolved in observer vehicle axes, meters

X+,X- translation forward, translation aft, respectively

Y+,Y- translation right, translation left, respectively

Z+,Z- translation down, translation up, respectively

$x, \tau$ dummy variables of integration

z z-transform variable

$\alpha, \beta$ azimuth and elevation angles of target with respect to observer vehicle axes, radians

$\Delta$ forward finite-difference operator, dimensionless

$\nabla$ backward finite-difference operator, dimensionless

$\delta$ velocity perturbation variable, dimensionless

$\epsilon$ global error in angular momentum squared using Euler integration, dimensionless; also used as orthogonality error, dimensionless

$\epsilon_r$ local relative roundoff error

$\epsilon_{tr}$ local relative truncation error

$\zeta_g$ gyroscope damping ratio, dimensionless

$\eta$ angle between $\bar{l}$ and $\bar{\omega}$, radians

| | |
|---|---|
| $\theta+,\theta-$ | upward and downward pitch, respectively |
| $\Lambda$ | variable associated with gyroscope equation, radians/second |
| $\lambda,\tau$ | target azimuth and elevation angle with respect to local vertical axis system, radians |
| $\mu,\phi_R,\nu$ | Euler angles which specify orientation of scaled target model axes with respect to simulation laboratory analog of line-of-sight axes, radians |
| $\rho$ | displacement perturbation variable, dimensionless |
| $\phi+,\phi-$ | right and left roll, respectively |
| $\chi$ | angle between $\bar{\omega}$ and $\bar{L}$, radians |
| $\psi,\theta,\phi$ | Euler angles relating observer vehicle axes to target-centered local vertical system, radians |
| $\psi+,\psi-$ | right and left yaw, respectively |
| $\psi_c,\theta_c,\phi_c$ | attitude angle errors used in attitude control system, radians |
| $\psi_i,\theta_i,\phi_i$ | Euler angles relating observer vehicle axes to an inertial frame, radians |
| $\Omega$ | skew-symmetric matrix which relates components of a vector to their derivatives due to referencing a rotating reference frame (equivalent to $\bar{\omega}X$ operation), radians/second |
| $\omega$ | magnitude of $\bar{\omega}$, radians/second |
| $\omega_c$ | general characteristic frequency, radians/second |
| $\omega_g$ | gyroscope natural frequency, radians/second |
| $\omega_o$ | orbital angular rate for target reference orbit, radians/second |
| $\bar{\omega}$ | angular velocity vector of observer vehicle with respect to inertial frame, radians/second |

$\bar{\omega}_t$ angular velocity vector of target vehicle with respect to inertial frame, radians/second

$(\dot{\ })$ denotes time derivative, second$^{-1}$

$()_n$ evaluation at time $t = nh$, dimensionless

$()^T$ transpose operation, dimensionless

$\left[\xi\right]_\lambda$ transformation matrix of a simple rotation through any angle $\xi$ about $\lambda$-axis, dimensionless

$\left[-\xi\right]_\lambda$ the inverse and/or transpose of $\left[\xi\right]_\lambda$, dimensionless

$()^{(j)}$ jth derivative, second$^{-j}$; also jth difference

Axis systems:

$X_i, Y_i, Z_i$ an "inertial" system (origin at center of the earth $X_i Z_i$-plane defines orbit plane of target vehicle, $Z_i$ passing through perifocus and $Y_i$ in direction of orbital angular velocity)

X,Y,Z target local vertical system (a rotating system, origin at center of gravity of target, Z-axis through center of earth, XZ-plane lies in target orbit plane. X-axis points generally backward in target orbit)

$X_{T,b}, Y_{T,b}, Z_{T,b}$ principal axes through center of gravity of target ($X_{T,b}$ forward, $Z_{T,b}$ down, $Y_{T,b}$ completes the right-hand system, docking ring aft)

$X_{o,b}, Y_{o,b}, Z_{o,b}$ observer body-axis system (origin at center of gravity of the observer vehicle; $X_{o,b}$ out nose of vehicle (forward), $Y_{o,b}$ out right wing, $Z_{o,b}$ (down) completes right-hand system)

$X_{los}, Y_{los}, Z_{los}$ line-of-sight axis system (origin coincident with origin of observer body axes and $X_{los}$ passes through origin of target local vertical, $Y_{los}$ lies in the $X_{o,b}Y_{o,b}$-plane)

## PROBLEM DESCRIPTION

### Background Discussion

The physical systems considered in the analysis are those of a class of problems rather than of any specific problem in order to approach the widest possible degree of applicability. The physical systems of concern are those of manned and unmanned flight vehicles. The greatest variability of vehicle simulations lies in three parts: structural effects, the coordinates used for kinematical variables, and the type of control forces. The vehicles are considered as structurally rigid except in an example problem of a system of two elastically coupled rigid vehicles studied in the latter part of this report. The rotational kinematic variables chosen are, in most cases, relatively uniform, a wide variety being used in the translational kinematics. The direction cosines and the Euler parameters (unit quaternion) are considered as representations of rotations since they overlap most present-day simulations. The angular momentum components are used for the moment description, and they reduce to the angular rate equations for constant inertias. The translational variables are considered in the analysis only in very general terms. The applicability (or lack thereof) of the analysis of the translational motion to a specific problem is clarified in the section "Analysis." All statements apply to any flight-rigid vehicle simulation as long as the control forces are zero. The only control forces considered are derived from a reaction – jet control system. The complete analysis is then only for the real-time simulation of rigid vehicles with on-off control. However, inferences to other problems are made where possible.

In addition to the on-off control forces, the effects of a gravitational field are also considered. The class of orbital-rigid vehicles with on-off control can be characterized by the frequencies associated with the motion. These characteristics are low frequencies ($\approx 10^{-3}$ radian/sec) associated with the steady-state trajectory motion, moderate frequencies ($\approx 1$ radian/sec) in attitude maneuvers, and usually high frequencies ($\approx 10$ to $10^2$ radians/sec) in the attitude-control system. After the analysis, two examples are taken from this class. The first is a Gemini-Agena rendezvous and station-keeping problem (ref. 11), the mathematical model of which is in appendix A. The second is a variation of this problem which includes an elastic tether (ref. 12). Also discussed are recent applications of the results of this analysis to several large simulations, some of which include aerodynamics.

### Fundamental Differential Equations

Associated with every manned vehicle is a set of fundamental differential equations, the solutions of which yield the vehicle's orientation, angular rates, position, and velocities. The description of differing vehicles mainly changes the coefficients and the inhomogeneous term (including the control system) of these fundamental equations.

Axis transformations.- Two methods of computing the transformation matrix are commonly used, both of which are considered in the analysis. These methods use the direction cosine rate equations and the Euler parameter rate equations.

The first and probably the most common method is use of the direction cosine rate equations. The nine direction cosine rate equations are partitioned into three related sets all of the form

$$\begin{bmatrix} \dot{l} \\ \dot{m} \\ \dot{n} \end{bmatrix} = \begin{bmatrix} 0 & r & -q \\ -r & 0 & p \\ q & -p & 0 \end{bmatrix} \begin{bmatrix} l \\ m \\ n \end{bmatrix} \tag{1}$$

Each related set has the property of normality

$$Q = l^2 + m^2 + n^2 = 1 \tag{2}$$

which is a constant of the motion.

Equation (1) can be written as

$$\dot{\bar{l}} = \Omega \bar{l} \tag{3}$$

where $\bar{l}$ is the vector of components $l$, m, and n and $\Omega$ is the skew-symmetric matrix in equation (1).

The Euler parameters are obtained from the following matrix differential equation (eqs. (A35) to (A39) with $K_\epsilon = 0$)

$$\begin{bmatrix} \dot{a} \\ \dot{b} \\ \dot{c} \\ \dot{d} \end{bmatrix} = \frac{1}{2} \begin{bmatrix} 0 & r & -q & -p \\ -r & 0 & p & -q \\ q & -p & 0 & -r \\ p & q & r & 0 \end{bmatrix} \begin{bmatrix} a \\ b \\ c \\ d \end{bmatrix} \tag{4}$$

Equation (4) can be written as

$$\dot{\bar{A}} = S\bar{A} \tag{5}$$

where $\bar{A}$ is the vector (a, b, c, and d) and S is the skew-symmetric matrix in equation (4) including the factor $\frac{1}{2}$. The orthonormality condition is (eq. (A39) for $\epsilon = 0$)

$$P = a^2 + b^2 + c^2 + d^2 = 1 \tag{6}$$

Hence, $P$ given by equation (6) is a constant of motion.

Attitude control system.- The simulation of the attitude control system is comprised of computing angles from the gyroscope outputs:

$$\left.\begin{aligned} \dot{\phi}_c &= p_g \\ \dot{\theta}_c &= q_g \\ \dot{\psi}_c &= r_g \end{aligned}\right\} \tag{7}$$

where $p_g$, $q_g$, and $r_g$ are the measured body angular rates and are usually given by the approximate linear gyroscope equations:

$$\left.\begin{aligned} \ddot{p}_g + 2\zeta_g\omega_g\dot{p}_g + \omega_g{}^2 p_g &= \omega_g{}^2 p \\ \ddot{q}_g + 2\zeta_g\omega_g\dot{q}_g + \omega_g{}^2 q_g &= \omega_g{}^2 q \\ \ddot{r}_g + 2\zeta_g\omega_g\dot{r}_g + \omega_g{}^2 r_g &= \omega_g{}^2 r \end{aligned}\right\} \tag{8}$$

where $p$, $q$, and $r$ are the true body angular rates as calculated from the moment equations.

Moment equations.- The moment or angular momentum rate equations are written as the following matrix equation (eqs. (A43) to (A45))

$$\begin{bmatrix} \dot{L}_1 \\ \dot{L}_2 \\ \dot{L}_3 \end{bmatrix} = \begin{bmatrix} 0 & r & -q \\ -r & 0 & p \\ q & -p & 0 \end{bmatrix} \begin{bmatrix} L_1 \\ L_2 \\ L_3 \end{bmatrix} + \begin{bmatrix} M_1 \\ M_2 \\ M_3 \end{bmatrix} \tag{9}$$

where from equations (A40) to (A42),

$$\begin{bmatrix} p \\ q \\ r \end{bmatrix} = \begin{bmatrix} I_{11} & I_{12} & I_{13} \\ I_{21} & I_{22} & I_{23} \\ I_{31} & I_{32} & I_{33} \end{bmatrix}^{-1} \begin{bmatrix} L_1 \\ L_2 \\ L_3 \end{bmatrix} \tag{10}$$

Equations (9) and (10) can be written as

$$\dot{\overline{L}} = \Omega\overline{L} + \overline{M} \tag{11}$$

and

$$\overline{\omega} = I^{-1}\overline{L} \tag{12}$$

Forming the scalar product with $\overline{L}^T$ and equation (11) yields

$$\overline{L}^T\dot{\overline{L}} = \overline{L}^T\Omega\overline{L} + \overline{L}^T\overline{M} \tag{13}$$

When $\overline{M}$ is null, the right-hand side of equation (13) vanishes since $\overline{L}$ is orthogonal to $\Omega\overline{L}$. This relation implies that $N$ (the total angular momentum squared) given by equation (14) is a constant of the motion for $\overline{M}$ null:

$$N = \overline{L}^T\overline{L} \tag{14}$$

Translational equations.- The translational equations are found in appendix A (eqs. (A4) to (A10)). They are characterized by very low frequencies $(\omega_c \approx 10^{-3}$ radian/sec) for nonthrusted motion. For thrusted motion, the frequencies become moderately high ($\omega_c \approx 1$ radian/sec from rotational motion coupling) but have little effect on the solution character. (The effect is a small-amplitude oscillation with $\omega_c \approx 1$ radian/sec modulated with a large-amplitude oscillation with $\omega_c \approx 10^{-3}$ radian/sec). The constants of motion for no thrust would be the total energy and orbital angular momentum.

## ANALYSIS

The errors considered in the analysis are of two types: the error introduced by using a finite-word structure (round-off error), and the error in using approximate formulas for limiting processes such as integration or differentiation (truncation error). The following sections begin with a discussion of local round-off and truncation error. These local errors are related to the accumulated or propagated error by error dominance. The concept of error dominance and its region applicability are discussed in the next section. Error dominance is then the guide to the analysis of the equations of motion. The analysis of each related set of equations is followed by a discussion of the results of experiment. Before beginning this task, it first seems advisable to establish the ground rules under which the analysis is performed.

Characteristic of any nontrivial simulation problem is the evaluation of many complicated algebraic expressions for visual display drives, readout, and the derivatives of the systems variables. The performance of the integration is, with few exceptions, the minor part of the computation (only a few arithmetic operations per integration). Hence, integration schemes which require the least number of derivative evaluations per integration interval are desirable (that is, multistep methods are preferred over the single-step methods). Equally important is the need to minimize the number of integration steps needed to obtain the problem solution (thus, the arithmetic unit is used as little as possible per problem second). Clearly, the interval size is to be made as large as possible in order to reduce the amount of computation required and small enough to provide "proper" response to the pilot input. Reference 13 indicates that intervals on the order of 100 milliseconds is adequate for sampling pilot input. However, the increased accuracy for smaller intervals is not clear because of roundoff error in that study. (The maximum word length was 7 bits.) For the remainder of this report, the maximum interval is assumed to be 50 milliseconds or 20 samples per second which should be more than adequate. (This sample rate is a factor of 2 more often than that suggested by ref. 13.) The minimum interval size is limited by the roundoff error and is discussed later in this report.

Two methods are used to study the propagated truncation error. The z-transforms (ref. 14) are used to study the linear portions of the problem. The changes in the constants of motion are also used to indicate the amount of error introduced in the problem solution by various integration schemes.

## Roundoff and Truncation

Analytical development.- The errors of numerical computation are of two classes: errors due to representing numbers by a finite word size (that is, roundoff) and errors due to neglecting higher order terms in approximate techniques (that is, truncation). Although the effects due to truncation can, more or less, be determined, the propagated error associated with round-off can seldom be rigorously studied for practical problems. Rather, the propagated roundoff error is studied through model building and experimentation. (See ref. 15, p. 41; ref. 16, p. 305.)

The equations of motion are approximated (in most cases) by finite difference equations of at least the same order of the equations of motion for consistency. (See ref. 15, p. 224.) Any finite-difference approximation of order greater than the order of the equations of motion introduces extraneous roots. (The language of linear equations is used here; the meaning should be clear.) In addition to the extraneous roots are other roots which approach the true roots of the differential equation in the limit as the interval approaches zero (that is, $h \rightarrow 0$) so that $nh$ is finite and equal to $t$. If the extraneous

roots are unstable (ref. 15, pp. 185, 242), the approximate solution is sensitive to small errors (for example, starting error or roundoff error) introduced in the calculation. (See ref. 17, p. 11.) This sensitivity (called numerical instability) usually occurs when the sample rate and the systems frequencies are of the same order of magnitude.

Implicit in the following sections is the assumption of numerical stability from which follows the concept of error dominance. Error dominance can be stated as follows: The propagated error will be dominated by $\left\{\begin{matrix}\text{roundoff} \\ \text{truncation}\end{matrix}\right\}$ error if, in the region of numerical stability, the local $\left\{\begin{matrix}\text{roundoff} \\ \text{truncation}\end{matrix}\right\}$ error is in magnitude much larger than the local $\left\{\begin{matrix}\text{truncation} \\ \text{roundoff}\end{matrix}\right\}$ error. This definition leaves an uncertain region between these regions where local roundoff and truncation error are within an order of magnitude of each other. Hence, these local errors compete in forming the propagated error.

In subsequent sections, error dominance is used to determine the error that is most likely to affect the solution. The equations of motion are then analyzed on this basis and compared with experimental results. However, the magnitude of the local relative roundoff and truncation errors must be determined first.

The local roundoff error is subdivided into two components, as in reference 15 (p. 36), the inherent error and the induced error. Extensive discussions of these errors are given in reference 15 and are not repeated here. Instead, a few simple notions about roundoff error are given and the reference is cited for a more extensive discussion. For the purpose at hand, the inherent error can be considered as the error in evaluating the derivatives of the system. Upon integration these errors are reduced in magnitude by the integration interval $h$. The induced error is introduced through the actual performance of the integration and is not reduced by $h$ but is always of the order of the least significant bit of the finite word structure (ref. 15, p. 35).

Before deriving an approximate model for the local relative roundoff and truncation error, consider a few simple operations in a hypothetical normalized 9-digit floating-point decimal machine. The word structure for a number is represented schematically as

$$A = (.aaaaaaa. \ldots) \times 10^{EXP_A}$$

$$0.1 \leqq A \times 10^{-EXP_A} < 1$$

where the $a$ terms are digits of values 0 to 9 and $EXP_A$ is the integer exponent of $A$. The decimal machine word structure is represented as

| $EXP_A$ | .aaaaaaaaa |
|---|---|

for a 9 significant digit machine. Note that the relative error of this machine representation of A is bounded by $10^{-9}$ (the relative value of the first significant digit being neglected by the decimal machine). The inherent error can largely be controlled by careful programing. Taking differences of nearly equal numbers results in a large inherent error, which is demonstrated schematically as follows:

| A = | EXP | .XXXXYYYYY |
|---|---|---|

| B = | EXP | .XXXXZZZZZ |
|---|---|---|

| A - B = | EXP - 4 | .DDDDDRRRR |
|---|---|---|

Roundoff

$$D = Y - Z$$

The roundoff error represented by the R digits move into the register when left shift is performed after subtraction. Thus, if this operation or similar ones are used, the inherent error may be significant. With careful programing, the inherent error can be neglected because of reduction by the interval h upon integration.

If it is assumed that the inherent error is controlled, the induced error must be studied. The source of the induced error resulting from a simple numerical integration procedure is shown as follows:

| $X_n$ = | $EXP_X$ | .XXXXXXXXX |
|---|---|---|

| $\dot{X}_n$ = | $EXP_{\dot{X}}$ | .$\dot{X}\dot{X}\dot{X}\dot{X}\dot{X}\dot{X}\dot{X}\dot{X}\dot{R}\dot{R}$ |
|---|---|---|

Inherent error

| h = | $EXP_h + 1$ | .100000000 |
|---|---|---|

| $\Delta X_n = h\dot{X}_n$ = | $EXP_{\dot{X}} + EXP_h$ | .$X_\Delta X_\Delta X_\Delta X_\Delta X_\Delta X_\Delta X_\Delta R_\Delta R_\Delta$ |
|---|---|---|

Shift right on $\Delta X_n$ exponent until equal to the $X_n$ exponent. Then add:

$$X_n + \Delta X_n = \boxed{EXP_X \mid .XXXXXXXXX}$$

Induced error

$$+ \boxed{EXP_X \mid .000000X_\Delta X_\Delta X_\Delta} \; \boxed{X_\Delta X_\Delta X_\Delta X_\Delta R_\Delta R_\Delta}$$

No. of zeroes = $EXP_X - EXP_{\dot{X}} - EXP_h$

Inherent error

$$= \boxed{EXP_X \mid .XXXXXXX_N X_N X_N}$$

$$X_N = X + X_\Delta$$

The variables $X_i$, $\dot{X}_i$, and $h$ are shown (with the inherent error in $\dot{X}$) in their decimal word representation. $\left(h = 10^{EXP_h}\right.$ is assumed for simplicity.$\left.\right)$ The integration is performed by (Euler integration is used for simplicity)

$$X_{n+1} = X_n + h\dot{X}_n$$

$$X_{n+1} = X_n + \Delta X_n$$

as shown schematically. The $\Delta X$ is computed, and is followed by a shift right (usually) until the exponents of $X$ and $\Delta X$ are the same. The addition is then performed. Note that the induced error is that part of the $\Delta X$ word shifted out of the register. Thus, the relative weight of the induced error in $X$ is always $10^{-9}$ (the relative weight of the rounded digit).

The control of the induced error could be performed by using a longer register and partial double precision as follows:

$$X_n = \boxed{EXP_X \mid .XXXXXXXXX \,\|\, XXXXXXXXX}$$

$$\dot{X}_n = \boxed{EXP_{\dot{X}} \mid .\dot{X}\dot{X}\dot{X}\dot{X}\dot{X}\dot{X}\dot{X}\dot{X}\dot{R}\dot{R}}$$

$$h = \boxed{EXP_h + 1 \mid .100000000}$$

$$\Delta X_n = h\dot{X}_n = \left| \text{EXP}_{\dot{X}} + \text{EXP}_h \right| .X_\Delta X_\Delta X_\Delta X_\Delta X_\Delta X_\Delta X_\Delta R_\Delta R_\Delta$$

Shift right on $\Delta X_n$ exponent until equal to the $X_n$ exponent and then add

$$X_n + \Delta X_n = \boxed{\text{EXP}_X \mid .XXXXXXXXX \parallel XXXXXXXXX}$$

Induced error

$$+ \boxed{\text{EXP}_X \mid .000000X_\Delta X_\Delta X_\Delta \parallel X_\Delta X_\Delta X_\Delta X_\Delta R_\Delta R_\Delta \mid RRR}$$

Inherent error

$$= \boxed{\text{EXP}_X \mid .XXXXXXX_N X_N X_N \parallel X_N X_N X_N X_N R_N R_N R_N' R_N' R_N'}$$

$$X_N = X + X_\Delta$$

The inherent error is

$$R_N = X + R_\Delta$$

The induced error is

$$R_N' = X + R$$

The register containing X, if sufficiently increased in length, would contain mainly the inherent error reduced by the integration interval size h. The derivatives $\dot{X}$ may still be evaluated by using the normal word size and two words for X; this mode of operation (partial double precision, ref. 15, p. 94) normally reduces roundoff error significantly. Examples are shown later in the text.

In order to make effective use of error dominance, the relative magnitudes of the local roundoff and truncation errors are needed. It will henceforth be assumed that good programing practices are followed and the inherent error can be neglected. A simple model is derived for the local relative roundoff and truncation error (inherent error being neglected) for second-order integration techniques and a normalized N-bit floating-point machine (binary).

It is assumed that the jth derivative of the state variables of the system are given by the relation

$$X^{(j)} = \omega_c{}^j X \tag{15}$$

where the characteristic frequency $\omega_c$ is, in general, complex.

Consider a Taylor series expansion of $X$ from the point $t = nh$ to $t = (n + 1)h$

$$X_{n+1} = X_n + h\dot{X}_n + \frac{1}{2} h^2 \ddot{X}_n + \frac{1}{6} h^3 \dddot{X}_n + \ldots . \tag{16}$$

Substituting equation (15) into equation (16) results in

$$X_{n+1} = \left(1 + h\omega_c + \frac{1}{2} h^2 \omega_c{}^2 + \frac{1}{6} h^3 \omega_c{}^3 + \ldots .\right) X_n \tag{17}$$

The solution using second-order integration is

$$X_{n+1} = \left(1 + h\omega_c + \frac{1}{2} h^2 \omega_c{}^2\right) X_n \tag{18}$$

and the local truncation error $T$ is

$$T \approx \frac{1}{6} h^3 \omega_c{}^3 X_n + O\left(h^4\right) \tag{19}$$

The change in $X$ to second order relative to $X$ is

$$\frac{1}{X_n} \Delta X_n = h\omega_c \left(1 + \frac{1}{2} h\omega_c\right) \tag{20}$$

which is approximately the change at the nth step of the normalized portion of the computer word representing $X$ since $X_n \approx 2^{EXP_X}$. Because of the finite word structure of the machine, the relative change in $X$ to second order is approximated in the calculations by

$$\left(\frac{\Delta X_n}{X_n}\right)_A \approx h\omega_c \left(1 + \frac{1}{2} h\omega_c\right) \pm 2^{-N_b - 1} \tag{21}$$

where $N_b$ is the number of significant binary bits. Hence, the local roundoff error $R$ is bounded by

$$-2^{-N_b-1} \left|X_n\right| \leq R \leq 2^{-N_b-1} \left|X_n\right| \tag{22}$$

The magnitude of the local relative roundoff error $\epsilon_r$ is defined as

$$\epsilon_r = \frac{|R|}{|\Delta X_n|} \tag{23}$$

which has a maximum of

$$\epsilon_r = \frac{2^{-N_b-1}}{\left|h\omega_c\left(1 + \frac{1}{2}h\omega_c\right)\right|} \tag{24}$$

and is a measure of the greatest significant change in $X$ that can occur and still be deleted from the calculation due to rounding.

The magnitude of the local relative truncation error $\epsilon_{tr}$, the remainder $O(h^4)$ being neglected, is

$$\epsilon_{tr} = \frac{|T|}{|\Delta X_n|} = \frac{1}{6}\frac{\left|h^2\omega_c{}^2\right|}{\left|\left(1 + \frac{1}{2}h\omega_c\right)\right|} \tag{25}$$

The two local relative errors given by equations (24) and (25) are the limits of resolution imposed on $\dot{X}$ by the word structure and integration scheme, respectively, as seen by the variable $X$.

In closing this section, it seems instructive to indicate the effects of statistical modeling on the local relative roundoff error. Two commonly used models for the distribution of roundoff error is to assume that roundoff is uniformly distributed or Gaussian distributed. Implicitly assumed is that roundoff error at the nth step is independent of the error at the previous steps. The uniform distribution is over the interval $(0,\epsilon_r)$ and the 50 percentile occurs at the midpoint, namely $1/2\epsilon_r$. That is, 50 percent of the errors will be less than $1/2\epsilon_r$ for the assumed uniform distribution. The 50 percentile for the Gaussian distribution occurs at 0.68STD (STD is the standard deviation) where $\epsilon_r$ = 4STD is assumed. The 50 percentile point is then $0.17\epsilon_r$.

Discussion of applications.- The models for the local relative roundoff and truncation error were derived by assuming the state variables of the system and their derivatives were linearly related. This assumption implies that the system has a degree of smoothness in its motion so that over short intervals of time (on the order of $h$), the motion is quadratic. The degree of variation of the characteristic frequency as a function

of the state variables and time clearly determines the validity of this local model. Discontinuities that arise from thrust destroys this linear relationship and this difficulty will be dealt with later in the section "Moment Equations."

The approximate local relative roundoff (the upper bound $\epsilon_r$; the uniform 50 percentile $\epsilon_r{}^U$; and the Gaussian 50 percentile $\epsilon_r{}^G$) and truncation errors are shown in figure 2 for $N_b = 27$ bits. These local errors are estimates of magnitudes only and no information is supplied for additivity (which is machine and program dependent).

The manner in which these errors propagate is a more complex problem than this simple analysis can ascertain. However, this analysis does indicate that the error most likely to enter the problem (error dominance) and an estimate of an upper bound of the propagated error can be found. (See ref. 15, p. 36.)

As seen in figure 2 with $N_b = 27$ bits, the portion of the computation including the attitude-control system $\left(h\omega_c \approx 1\right)$ and moment equations and axis transformations $\left(h\omega_c \approx 10^{-2}\right)$ could be greatly affected by truncation with little concern for roundoff. If low-order integration schemes are to be used in these portions of the simulation, great care must be employed to determine any possible adverse effects. However, the translational equations $\left(h\omega_c \approx 10^{-5}\right)$ are relatively insensitive to truncation error but roundoff error could be a prime difficulty.

## Axis Transformations

Analytical development.- The transformation matrix is computed either directly by integrating the direction cosine rate equations or by the Euler parameter rate equations, both of which must be subject to the restrictions of orthonormality. By using the steepest descents, the rate equations could be augmented with constraints to maintain orthonormality. (For example, see eqs. (A35) to (A39).) Although orthonormality would be maintained, phasing errors could become appreciable. In this vein, an integration scheme is chosen that closely approximates the orthonormality condition. This scheme will then be used in conjunction with a normalization procedure to maintain orthogonality of the transformation matrix.

First consider Euler integration to solve the direction cosine rate equations given by equation (3)

$$\bar{l}_{n+1} = \bar{l}_n + h\dot{\bar{l}}_n = \bar{l}_n + h\Omega_n\bar{l}_n \tag{26}$$

The norm squared (eq. (2)) by using equation (26) becomes (where $\Omega\bar{l} = \bar{\omega}\mathrm{X}\bar{l}$)

$$Q_{n+1} = Q_n + h^2\left(\Omega_n \bar{l}_n\right)^T\left(\Omega_n \bar{l}_n\right) = Q_n + \left(h\omega_n \sin \eta_n\right)^2 Q_n \tag{27}$$

where $\eta_n$ is the angle between the $\bar{l}_n$ and the $\bar{\omega}_n$ at $t = nh$. From equation (27), the per step error due to Euler integration is

$$\Delta Q_n = \left(h\omega_n \sin \eta_n\right)^2 Q_n \tag{28}$$

Similarly, the Adams-Bashforth integration formula yields

$$\bar{l}_{n+1} = \bar{l}_n + \frac{h}{2}\left(3\Omega_n \bar{l}_n - \Omega_{n-1}\bar{l}_{n-1}\right) \tag{29}$$

and the per step error of the norm is

$$\Delta Q_n = -h\bar{l}_n^T \Omega_{n-1}\bar{l}_{n-1} + \frac{h^2}{4}\bar{U}^T\bar{U} \tag{30}$$

where

$$\bar{U} = 3\Omega_n \bar{l}_n - \Omega_{n-1}\bar{l}_{n-1}$$

A striking difference in the change of the norm is apparent for the two schemes, as seen in equations (28) and (30). Euler integration gives rise to a positive definite change in the norm as opposed to Adams-Bashforth integration which does not have a definite norm change. Hence, Euler integration always increases the norm for each integration step. For example, consider the ratio of the change in the norm squared to the norm squared with Euler integration for $h\omega \approx 10^{-2}$ radian

$$\frac{\Delta Q_n}{Q_n} \approx h^2\omega^2 \approx 10^{-4} = 0.01 \text{ percent}$$

Hence, an error of 0.01 percent is committed per integration step. Clearly, a solution for a reasonable length of time is not acceptable even for moderate frequencies ($\omega \approx 1$ radian/sec) and interval sizes $\left(h \approx 10^{-2} \text{ sec}\right)$.

Consider equation (27) when $\bar{\omega}$ is a constant. The z-transform of equation (27) is ($\sin \eta$ is also constant to a very good approximation)

$$\left(z - 1 - h^2\omega^2 \sin^2 \eta\right)Q(z) = 0 \tag{31}$$

which has one root

$$z = 1 + h^2\omega^2\sin^2\eta \tag{32}$$

The solution to equation (27) is then

$$Q_n = z^n = e^{n \log_e(z)} \tag{33}$$

By using the assumptions that

$$h^2\omega^2\sin^2\eta << 1 \tag{34}$$

and

$$\log_e(1 + X) \approx X - \frac{1}{2}X^2 + \frac{1}{3}X^3 - \frac{1}{4}X^4 \tag{35}$$

an approximate solution (the first nonvanishing term in approximation (35) being retained) for the norm squared is

$$Q \approx e^{h(\omega \sin \eta)^2 t} \tag{36}$$

when Euler integration is used.

The solution of the direction cosine rate equations for Euler integration is found by taking the z-transform of equation (26) with $\Omega$ a constant. The z-transformed equation can be written as

$$\left[(z - 1)I - h\Omega\right]\bar{l}(z) = 0$$

where the identity matrix $I$ in this and similar equations is suppressed in the sequel. Hence, the equation is written

$$\left[(z - 1) - h\Omega\right]\bar{l}(z) = 0 \tag{37}$$

The characteristic equation of equation (37) is

$$(z - 1)\left[(z - 1)^2 + h^2\omega^2\right] = 0 \tag{38}$$

for which

$$\left.\begin{aligned} z_1 &= 1 \\ z_{2,3} &= 1 \pm i\omega h \end{aligned}\right\} \tag{39}$$

are solutions.

The solution to equation (26) is then

$$\bar{l}_n = \bar{c}_1 + \bar{c}_2 e^{n \log_e(1+i\omega h)} + \bar{c}_3 e^{n \log_e(1-i\omega h)} \tag{40}$$

where the $\bar{c}_j$ terms are constant vectors that depend on initial conditions. Again with approximation (35) and by assuming that $|ih\omega| << 1$, equation (40) is rewritten by retaining the first nonvanishing terms in damping and frequency errors as

$$\bar{l} = \bar{c}_1 + e^{h\frac{\omega^2}{2}t}\left[\bar{c}_2 e^{i\left(\omega - \frac{h^2\omega^3}{3}\right)t} + \bar{c}_3 e^{-i\left(\omega - \frac{h^2\omega^3}{3}\right)t}\right] \tag{41}$$

Equation (41) is in agreement with equation (36).

The solution for the direction cosines using Adams-Bashforth second-order integration is found by taking the z-transform of equation (29) for constant $\Omega$ (where the identity matrix is implied):

$$\left[z(z - 1) - \frac{h}{2}\Omega(3z - 1)\right]\bar{l}(z) = 0 \tag{42}$$

The characteristic equation of equation (42) is

$$z(z - 1)\left\{\left[z(z - 1)\right]^2 + \frac{h^2}{4}\omega^2(3z - 1)^2\right\} = 0 \tag{43}$$

Two roots of equation (43) are by inspection:

$$z_1 = 0 \tag{44}$$

$$z_2 = 1 \tag{45}$$

and the four other roots are given by

$$\left[z(z - 1)\right]^2 = -c^2(3z - 1)^2 \tag{46}$$

where $c = \frac{h}{2}\omega$. Equation (46) can be reduced by taking the square root of each side:

$$z(z - 1) = \pm ic(3z - 1) \tag{47}$$

The roots of equation (47) are then given by

$$\left.\begin{aligned} z_{3,5} &= \frac{1}{2}\left\{(1 - i3c) \pm \left[\left(1 - 9c^2\right) - i2c\right]^{1/2}\right\} \\ z_{4,6} &= \frac{1}{2}\left\{(1 + i3c) \pm \left[\left(1 - 9c^2\right) + i2c\right]^{1/2}\right\} \end{aligned}\right\} \tag{48}$$

The four roots represented by equation (48) are two sets of complex conjugate pairs. This fact can be verified by substituting -i for i.

The real and imaginary parts of the roots given by equation (48) are found by defining

$$ue^{i\sigma} = \left(1 - 9c^2\right) + i2c$$

It is seen from this definition that

$$u^{1/2}e^{i\sigma/2} = \left[\left(1 - 9c^2\right) + i2c\right]^{1/2}$$

$$u^{1/2}e^{-i\sigma/2} = \left[\left(1 - 9c^2\right) - i2c\right]^{1/2}$$

where

$$u = \left(1 - 14c^2 + 81c^4\right)^{1/2} \tag{49}$$

$$\sigma = \tan^{-1}\left(\frac{2c}{1 - 9c^2}\right) \tag{50}$$

Hence, the roots given by equation (48) are

$$\left.\begin{aligned} z_{3,4} &= \frac{1}{2}\left[\left(1 + u^{1/2}\cos\frac{\sigma}{2}\right) \pm i\left(3c + u^{1/2}\sin\frac{\sigma}{2}\right)\right] \\ z_{5,6} &= \frac{1}{2}\left[\left(1 - u^{1/2}\cos\frac{\sigma}{2}\right) \pm i\left(3c - u^{1/2}\sin\frac{\sigma}{2}\right)\right] \end{aligned}\right\} \tag{51}$$

If $c \ll 1$ is assumed $\left(\text{for } c = \frac{h\omega}{2} \approx 10^{-2} \text{ radian}\right)$, equations (49) and (50) can, terms in $c^5$ and higher being neglected, be approximated by

$$u = 1 - 7c^2 + 16c^4 \tag{52}$$

$$\sigma = 2c\left(1 + \frac{23}{3}c^2\right) \tag{53}$$

and similarly

$$u^{1/2} = 1 - \frac{7}{2}c^2 + \frac{15}{8}c^4 \tag{54}$$

$$\sin\frac{\sigma}{2} = c\left(1 + \frac{45}{6}c^2\right) \tag{55}$$

$$\cos\frac{\sigma}{2} = 1 - \frac{1}{2}c^2 - \frac{61}{8}c^4 \tag{56}$$

Substituting equations (54), (55), and (56) into equations (51) results in

$$z_{3,4} \approx 1 - 2c^2 - 2c^4 \pm i\left(2c + 2c^3\right) \tag{57}$$

$$z_{5,6} \approx 2c^2 + 2c^4 \pm i\left(c - 2c^3\right) \tag{58}$$

The two roots given by equation (58) are quickly damped for $h\omega$ small or equivalently for $c$ small. If the heavily damped roots are neglected and approximation (35) is used, the solution of the direction cosines for the Adams-Bashforth second-order integration scheme is given as

$$\bar{l} \approx \bar{c}_1 + e^{4\frac{h^3\omega^4}{16}t}\left[\bar{c}_2 e^{i\left(\omega+\frac{5}{12}h^2\omega^3\right)t} \quad \bar{c}_3 e^{-i\left(\omega+\frac{5}{12}h^2\omega^3\right)t}\right] \tag{59}$$

where $\bar{c}_1$, $\bar{c}_2$, and $\bar{c}_3$ are the same as in equation (41). By comparing the solution given by equation (59) to that given by equation (41), the solution for the norm squared for Adams-Bashforth integration is by analogy with equation (36)

$$Q \approx e^{8\frac{h^3\omega^4}{16}(\sin\eta)^2 t} \tag{60}$$

when second-order Adams-Bashforth integration is used.

In order to make comparisons of the direction cosine formulation with the Euler parameter formulation, the Euler parameter rate equations will now be solved under the two integration schemes. Note that the z-transformed characteristic equations (eqs. (32) and (43)) are often similar in form so that the factors already obtained can be used in the following analysis and will reappear in later sections.

If Euler integration is applied to equations (5) and (6),

$$\bar{A}_{n+1} = \bar{A}_n + hS_n\bar{A}_n \tag{61}$$

$$\Delta P_n = \frac{h^2\omega_n^2}{4} P_n \tag{62}$$

From equation (62) for $\bar{\omega}$ constant,

$$P \approx e^{h\frac{\omega^2}{4}t} \tag{63}$$

which is the same result as that obtained from the solution of equation (61)

$$\bar{A} = e^{\frac{h\omega^2}{8}t}\left[\bar{a}_1 e^{i\left(\frac{\omega}{2} - \frac{h^2\omega^3}{24}\right)t} + \bar{a}_2 e^{-i\left(\frac{\omega}{2} - \frac{h^2\omega^3}{24}\right)t}\right] \tag{64}$$

where again approximation (35) has been used and only the lowest nonvanishing order in amplitude and frequency errors has been retained. The $\bar{a}_i$ terms are constant vectors that depend on the initial conditions.

Similarly, for Adams-Bashforth second-order integration,

$$\bar{A}_{n+1} = \bar{A}_n + \frac{h}{2}\left(3S_n\bar{A}_n - S_{n-1}\bar{A}_{n-1}\right) \tag{65}$$

$$\Delta P_n = -h\bar{A}_n{}^T S_{n-1}\bar{A}_{n-1} + \frac{h^2}{4}\left(3S_n\bar{A}_n - S_{n-1}\bar{A}_{n-1}\right)^2 \tag{66}$$

Again, the solution of equation (65) is found by z-transforms for $\bar{\omega}$ a constant (that is, S is constant).

$$\left[z(z-1) - \frac{h}{2}S(3z-1)\right]\bar{A}(z) = 0 \tag{67}$$

where the identity matrix is implied. By letting $c = \frac{h\omega}{4}$, the characteristic equation of equation (67) can be written as

$$\left[z^2(z - 1)^2 + c^2(3z - 1)^2\right]^2 = 0 \tag{68}$$

which is of the same form as equation (46). Hence, the roots are of the form of equations (57) and (58) where again the roots of equation (58) are heavily damped. The solution of equation (65), the heavily damped roots being neglected, is approximated by

$$\overline{A} = e^{4\frac{h^3\omega^4}{256}t}\left[\bar{a}_1 e^{i\left(\frac{\omega}{2}+\frac{5}{96}h^2\omega^3\right)t} + \bar{a}_2 e^{-i\left(\frac{\omega}{2}+\frac{5}{96}h^2\omega^3\right)t}\right] \tag{69}$$

where the $\bar{a}_i$ terms are the same as those in equation (64). From equation (69), the solution for the norm squared for Adams-Bashforth second-order integration (eq. (66)) is found to be

$$P \approx e^{8\left(\frac{h^3\omega^4}{256}\right)t} \tag{70}$$

Discussion of experiment.- The results of this analysis are summarized in table I. The growth time constants and frequencies for both the direction cosines and Euler parameters when Euler and Adams-Bashforth second-order integration are used are compared with the parameters of the corresponding differential equations.

The effects of the truncation error (hence, the propagated truncation error) for the direction cosine and Euler parameter rate equations has been determined for constant $\overline{\omega}$. In all cases it is seen that frequency of the system is only slightly affected. The most prominent behavior (for $\overline{\omega}$ constant) is seen to be the amplitude growth which is reflected in the norm.

The solutions to the norm of the direction cosine and Euler parameter rate equations using Euler and Adams-Bashforth integration were obtained both analytically and on the computer. Euler integration was used to start the Adams-Bashforth scheme. The solutions were obtained for

$$p = q = r = \frac{1}{\sqrt{3}}\ \frac{\text{radians}}{\text{second}}$$

$$\sin \eta = 1$$

initially and

$$h = \frac{1}{16} \text{ second}$$

These solutions were compared with the true norm which is unity and the resultant errors are shown in figures 3 to 6. As seen in these figures, the solution parameters as given by table I are accurate. (Also shown are the starting errors caused by the Euler integration starting formula.)

The solution parameters in table I clearly show that the Adams-Bashforth second-order integration and the Euler parameters are superior to the other possible combinations. The time constant is better by a factor of 16 and the frequency error is also the smallest. This combination is sufficient for many simulation problems as witnessed also in figure 6. (With $h = 2^{-4}$ sec, $|\overline{\omega}| = 1$ radian/sec for intervals of 100 seconds is more accurate than is required for most problems.) However, note that starting errors can be appreciable for nonzero p, q, and r when Euler integration is used to compute starting values.

The assumption that $\overline{\omega}$ is constant used in the analysis is not realistic. In general, $\overline{\omega}$ is a function of time with magnitude varying between zero and some $\omega_{max}$. When $\overline{\omega}$ is small, roundoff error will again affect the solution. The magnitude $|\overline{\omega}|$ is small during coasting periods of the flight where the control system is normally in attitude hold and the vehicle exhibits limit cycle motion inside a deadband. During this type of motion, roundoff error is the dominant error entering the solution. The main concern is placed on the stability of the limit cycle and usually the amount of fuel used during this portion of the flight. For most manned vehicles, the limit cycle motion is stable for a $N_b = 27$ bit machine for $h \geqq 15$ msec (this value is not a known absolute lower bound) and the experimental results are presented later.

The $\overline{\omega}$ is, in general, time varying and the analysis is not applicable. Euler integration has the property that the change in the norm is always positive definite (see eq. (28)) and is always unstable. The Adams-Bashforth second-order integration is not positive definite and the norm may actually decrease for time varying $\overline{\omega}$. (This effect is seen later in another section.)

Typically in flight simulation, attitude maneuvers are performed by sustaining some constant angular rate over a maximum time interval. An estimate of the adequacy of the two formulations can then be made by using the parameters in table I. One then has a basis for choosing a formulation and integration scheme for a particular application.

## Attitude Control System

Analytical development.- The response of the attitude-hold mode is strongly dependent on the quality of the solutions of equations (7) and (8), the attitude angle error, and the gyroscope outputs. If it is assumed that the solutions of equations (8) (the gyroscope outputs) are truly representative of the angular rates of the vehicles, conclusions can be made as to the integration scheme to be used for equations (7). Consideration is only given to the first of equations (7)

$$\dot{\phi}_c = p_g \tag{71}$$

since the analysis holds for the $\dot{\theta}_c$ and $\dot{\psi}_c$ equations as well.

For an on-off attitude control moment, the angular rate is approximated by

$$p_g \approx \frac{1}{I_{11}} \int M_1 \, dt \tag{72}$$

The moment of inertia is a slowly varying function of time; hence, over short-time intervals it may be considered to be constant. Since $M_1$ is either zero or a constant, the rate given by equation (72) is a constant or linear function of time, respectively. Visually,

$$p_g = p_{g,o} + \left(\frac{M_1}{I_{11}}\right) t \tag{73}$$

where the $t$ coefficient is zero or a constant value and the subscript $o$ denotes initial conditions. The solution to equation (71) is either a linear $\left(M_1 = 0\right)$ or quadratic $\left(M_1 \neq 0\right)$ function of time, as

$$\phi_c = \phi_{c,o} + p_{g,o} t + \left(\frac{1}{2} \frac{M_1}{I_{11}}\right) t^2 \tag{74}$$

Consider Adams-Bashforth Lth-order integration as applied to equation (71)

$$\phi_{c_{n+1}} = \phi_{c_n} + h \sum_{j=0}^{L-1} \gamma_j \nabla^j p_{g,n} \tag{75}$$

where the $\gamma_j$ values are given in reference 15 (pp. 192-193). Since $p_g$ is at most a linear function of $t$, $L = 2$ in equation (75) is an exact representation of $\phi_c$ under

these assumptions (eqs. (73) and (74)). This relationship is true since all higher orders of $p_g$ vanish (ref. 18, p. 9).

The equation for $p_g$ is considered to be representative of equations (8).

$$\ddot{p}_g + 2\zeta_g\omega_g\dot{p}_g + \omega_g{}^2 p_g = \omega_g{}^2 p \tag{76}$$

The forcing function in equation (76) is a relatively smooth function of time. Even so, with typical parameters $\left(\omega_g \approx 10^2 \text{ radians/sec} \text{ and } \zeta_g \approx 0.8\right)$, the numerical solution of equation (76) is not well behaved for simple numerical techniques when a reasonable interval size $\left(h \approx 10^{-2} \text{ sec}\right)$ is used.

The solution to equation (76) has been the object of research for many investigators. Examples of these efforts are given in references 4 to 7. The results of several such studies are summarized in reference 5. In view of the conclusions of reference 5, the next matter to be considered in this paper is to derive a method by which equation (76) can be solved. The complete derivation is contained in appendix B and only the highlights appear in this section.

The solution to equation (76), as found in appendix B, is

$$p_g(t) = \int_0^t G(t - \tau)\, p(\tau)\, d\tau \tag{77}$$

where

$$G(\tau) = \frac{\omega_g{}^2}{\Gamma} e^{-\xi\tau} \sin \Gamma\tau \tag{78}$$

with

$$\Gamma = \left(1 - \zeta_g{}^2\right)^{1/2} \omega_g$$

$$\xi = \zeta_g\omega_g$$

and $G(\tau)$ is a solution of the equation

$$\ddot{G}(t - \tau) + 2\zeta_g\omega_g\dot{G}(t - \tau) + \omega_g{}^2 G(t - \tau) = \omega_g{}^2 \delta(t - \tau)$$

and $\delta(t - \tau)$ is the Dirac delta function. (See ref. 19, p. 255.) As shown in appendix B, the solution given by equation (77) is valid even when $p$ is a nonlinear function of $p_g$.

(p is a nonlinear function of $p_g$ for most control systems.) For further discussions of nonlinearities, see reference 20.

A step-by-step evaluation procedure for solving equation (77) is found to be (eqs. (B36))

$$\begin{bmatrix} p_g(t+h) \\ \Lambda(t+h) \end{bmatrix} = e^{-\xi h} \begin{bmatrix} \cos \Gamma h & \sin \Gamma h \\ -\sin \Gamma h & \cos \Gamma h \end{bmatrix} \begin{bmatrix} p_g(t) + \int_0^h G(-x)p(t+x)dx \\ \Lambda(t) + \int_0^h G^\dagger(-x)p(t+x)dx \end{bmatrix} \tag{79}$$

If $p(t)$ is known on the interval $(t, t+h)$, equations (79) could be evaluated exactly. In practice, $p(t)$ is known to the accuracy of the integration scheme used to obtain it. Assume that $p(t)$ is known to within a linear function (Euler integration) on $(t, t+h)$ (see eq. (73))

$$p(t+x) = a + bx \tag{80}$$

where $0 \leqq x \leqq h$ and $a$ and $b$ are constants over the interval that depend on $p(t)$ and its derivatives. By substitution of equation (80) into equations (79), equations (79) can be written as

$$\begin{bmatrix} p_g(t+h) \\ \Lambda(t+h) \end{bmatrix} = e^{-\xi h} \begin{bmatrix} \cos \Gamma h & \sin \Gamma h \\ -\sin \Gamma h & \cos \Gamma h \end{bmatrix} \begin{bmatrix} p_g(t) + aI_1 + bI_2 \\ \Lambda(t) + aI_1^\dagger + bI_2^\dagger \end{bmatrix} \tag{81}$$

where

$$\left.\begin{aligned} I_1 &= \int_0^h G(-x)dx \\ I_2 &= \int_0^h G(-x)x\,dx \\ I_1^\dagger &= \int_0^h G^\dagger(-x)dx \\ I_2^\dagger &= \int_0^h G^\dagger(-x)x\,dx \end{aligned}\right\} \tag{82}$$

Evaluation of integrals (82) results in

$$\left.\begin{aligned} I_1 &= \frac{1}{\omega_g{}^2}\left[\xi G(-h) + \Gamma G^{\dagger}(-h)\right] - 1 \\ I_1{}^{\dagger} &= \frac{1}{\omega_g{}^2}\left[\xi G^{\dagger}(-h) - \Gamma G(-h)\right] - \frac{\xi}{\Gamma} \\ I_2 &= \frac{1}{\omega_g{}^2}\left[h\xi G(-h) + h\Gamma G^{\dagger}(-h) - \xi I_1 - \Gamma I_1{}^{\dagger}\right] \\ I_2{}^{\dagger} &= \frac{1}{\omega_g{}^2}\left[h\xi G^{\dagger}(-h) - h\Gamma G(-h) - \xi I_1{}^{\dagger} + \Gamma I_1\right] \end{aligned}\right\} \tag{83}$$

The integrals (82) are constants that need only be evaluated once and then used as coefficients in equations (81). For each interval step, only the coefficients a and b of equations (81) need to be evaluated. An obvious choice for a and b is

$$\left.\begin{aligned} a &= p(t) \\ b &= \dot{p}(t) \end{aligned}\right\} \tag{84}$$

However, more accurate approximations for b can be made; for example,

$$b = \frac{1}{2}\left[3\dot{p}(t) - \dot{p}(t - h)\right] \tag{85}$$

It is also a simple matter to make more accurate approximations to p(t) than that given by equation (80).

When gyroscopes are involved, a more accurate approximation for $\phi_c$ can be made than that given by equation (75). This approximation is made by integrating $p_g$ as given by equations (81) and expanding the results in a manner similar to this treatment.

Discussion of experiment.- The linear gyroscope equations were solved by using the Green's function technique for a step and ramp input. The parameters were $\omega_g = 125$ radians/sec, $\zeta_g = 0.8$, and $h = 1/64$ sec. The response, as seen in figures 7 and 8, were unchanged when the interval size was doubled. This result is expected since it is an analytical solution. Note that the solution even for discontinuities occurring at the beginning of the integration interval is still exact.

An independent study (ref. 8) has shown the $h \approx 10^{-4}$ sec (10 000 solutions per second) is required for the Adams-Moulton second-order method to obtain a reasonable solution. This requirement is obviously a difficult one for simulation in real time.

The Green's function technique employed to solve the gyroscope equations is exact when the forcing function is linear over the integration intervals. Higher order terms can be carried in approximating the forcing function with little added computer time. This method should be extended to include such effects as nonwindup limiting (piecewise linear gyroscope equations). This technique can also be extended to other linear and piecewise linear systems.

Recently, Giese (ref. 21) has used a similar method for solving the linear part of control systems. He has developed an algorithm for computing an approximate Green's function for the general case. Although the approximate Green's function is step size dependent as can be seen in figure 12 of reference 21, the algorithm approach is in the right direction. The Giese algorithm, however, does appear to have convergence problems as seen by comparing the results from second-order Adams-Bashforth solutions and the results of the Giese algorithm shown in figures 11 and 12, respectively, in reference 21.

## Moment Equations

Analytical development.- The analysis of the moment equations is accomplished in two steps. First considered is the case of no external torques for which the total angular momentum squared (eq. (14)) is a constant of the motion. This analysis is followed by a discussion of applied on-off control torques. Throughout the analysis, it is assumed that the angular momentum and angular velocity are measured in the principal axes. The inertia matrix and its inverse are then diagonal. This procedure greatly simplifies the analysis without loss of generality.

The moment equations are not linear. This nonlinearity is seen by writing the moment equations in component form, the angular velocity components being replaced by their functional form given by equation (12),

$$\left.\begin{aligned}
\dot{L}_1 &= rL_2 - qL_3 + M_1 = L_2L_3\left(\frac{1}{I_{33}} - \frac{1}{I_{22}}\right) + M_1 \\
\dot{L}_2 &= pL_3 - rL_1 + M_2 = L_3L_1\left(\frac{1}{I_{11}} - \frac{1}{I_{33}}\right) + M_2 \\
\dot{L}_3 &= qL_1 - pL_2 + M_3 = L_1L_2\left(\frac{1}{I_{22}} - \frac{1}{I_{11}}\right) + M_3
\end{aligned}\right\} \tag{86}$$

Although a solution to the general problem has not been found, two solutions have been approximated for two important types of vehicles. The first is vehicles with "near" cylindrical symmetry (that is, only two principal inertias are nearly equal), and the second is vehicles of "near" spherical symmetry (that is, all three inertias are nearly equal). For types of near cylindrical symmetry, the moment equations are approximately linear and z-transforms can be used. The moment equations are nonlinear for "near" spherical symmetry but an approximate solution can be found for the Euler integration scheme.

No external torques: The moment equations have the same form as the direction cosine rate equations for no external torques (that is, $M_1 = M_2 = M_3 = 0$). It follows that the per step error in the total angular momentum squared due to Euler and Adams-Bashforth second-order integration are, respectively,

$$\Delta N_n = h^2 \omega_n{}^2 N_n \sin^2 \chi_n \tag{87}$$

and

$$\Delta N_n = -h \bar{L}_n{}^T \dot{\bar{L}}_{n-1} + \frac{h^2}{4} \left( 3\dot{\bar{L}}_n - \dot{\bar{L}}_{n-1} \right)^2 \tag{88}$$

where $\chi_n$ is the angle between the $\bar{\omega}_n$ and $\bar{L}_n$ vectors. Again, the change due to Euler integration is positive definite and the Adams-Bashforth integration result is not positive definite.

Near cylindrical symmetry: Assume that the X-axis to be the axis of near symmetry, that is

$$I_{33} = I_{22} + \delta I \tag{89}$$

By using definition (89), equations (86) become, if first-order terms in $\delta I$ are retained:

$$\left.\begin{aligned} \dot{L}_1 &= -\frac{\delta I}{I_{22}{}^2} L_2 L_3 \\ \dot{L}_2 &= \left( -K + \frac{\delta I}{I_{22}{}^2} \right) L_3 L_1 \\ \dot{L}_3 &= K L_1 L_2 \end{aligned}\right\} \tag{90}$$

where $K = \frac{1}{I_{22}} - \frac{1}{I_{11}}$.

The near cylindrical symmetric approximation is used when

$$\left.\begin{aligned} |K| &>> \frac{|\delta I|}{I_{22}{}^2} \\ |\delta I| &<< I_{22} \end{aligned}\right\} \tag{91}$$

for which equations (90) degenerate to the equations of an oscillator since $\dot{L}_1 \approx 0$. Equations (90) become, in matrix form,

$$\begin{bmatrix} \dot{L}_2 \\ \dot{L}_3 \end{bmatrix} = \begin{bmatrix} 0 & KL_1 \\ -KL_1 & 0 \end{bmatrix} \begin{bmatrix} L_2 \\ L_3 \end{bmatrix} \tag{92}$$

with

$$KL_1 \approx KI_{11}p_o = p_o\left(1 - \frac{I_{11}}{I_{22}}\right) \tag{93}$$

where $p_o$ is a constant roll rate.

To analyze equations (92), the range of the quantity $KI_{11}$ needs to be determined. To accomplish this end, first observe that the inertias do not uniquely define the body configuration; that is, bodies of uniform material but with many different shapes can all have the same inertia matrix. Hence, perturbations from the set of all cylinders of uniform material are (dynamically) equivalent to the set of all nearly cylindrically symmetric bodies. Therefore, no generality is lost by considering perturbations of the cylindrical body of uniform material shown in figure 9; the inertias are (for $\delta I = 0$):

$$\left.\begin{aligned} I_{11} &= \frac{1}{2} mR^2 \\ I_{22} &= \frac{1}{12} m\left(3R^2 + l^2\right) \\ I_{33} &= I_{22} \end{aligned}\right\} \tag{94}$$

Where R and $l$ are as indicated in figure 9. Substituting equations (94) into equation (93) yields

$$KI_{11} \approx \frac{6}{3 + r^2} - 1 \tag{95}$$

where $r = \ell/R$ is the ratio of length to radius and always positive. Looking at the derivative of $K$ with respect to $r$

$$I_{11} \frac{dK}{dr} = \frac{-12r}{3 + r^2} < 0$$

reveals $KI_{11}$ to be a monotonic decreasing function of $r$ $(r > 0)$. The minimum and maximum values of $I_{11}K$ are at the maximum and minimum values of $r$. Looking at the limits of the rotating disk $(r \to 0)$ and rotating rod $(r \to \infty)$ establishes the limits of equation (95).

$$\left.\begin{aligned} \lim_{r \to 0} KL_1 &= p_o \\ \lim_{r \to \infty} KL_1 &= -p_o \end{aligned}\right\} \tag{96}$$

The general character of $I_{11}K$ is shown in figure 10. Consider a slight perturbation from cylindrical symmetry

$$I_{33} = I_{22} + \delta I$$

For the near cylindrical symmetric approximation to be valid

$$I_{22} \left| K \right| >> \frac{\left| \delta I \right|}{I_{22}}$$

but from equations (91),

$$I_{22} \left| K \right| = \frac{\left| I_{22} - I_{11} \right|}{I_{11}} >> \frac{\left| \delta I \right|}{I_{22}} \tag{97}$$

Hence, as shown by this relation, small perturbations from cylindrical symmetry for very long slender and/or short flat bodies do not greatly remove the motion from that of cylindrical symmetry since relation (97) is valid. However, as

$$\frac{\left| I_{22} - I_{11} \right|}{I_{11}} \to \frac{\left| \delta I \right|}{I_{22}}$$

the motion approaches a region where nonlinear motion resumes since the coefficients in equations (90) are then on the same order of magnitude $\left(\text{that is, } |K| \approx \frac{|\delta I|}{I_{22}^2}\right)$. Hence, figure 10 can be divided into two regions. Region I is where relation (97) is satisfied and the motion is nearly linear. Region II is where relation (97) is not satisfied and the motion is not described by the approximate equations (92). In region II is the class of bodies with near spherical symmetry.

For near cylindrical symmetry, the angular momentum rate equations are

$$\begin{bmatrix} \dot{L}_2 \\ \dot{L}_3 \end{bmatrix} = \begin{bmatrix} 0 & -k \\ k & 0 \end{bmatrix} \begin{bmatrix} L_2 \\ L_3 \end{bmatrix} \tag{98}$$

where $k = L_1 K$.

Consider the integration of equations (98) by using first the Euler integration and then the Adams-Bashforth second-order integration formula. For Euler integration,

$$\begin{bmatrix} L_2 \\ L_3 \end{bmatrix}_{n+1} - \begin{bmatrix} L_2 \\ L_3 \end{bmatrix}_n = h \begin{bmatrix} 0 & -k \\ k & 0 \end{bmatrix} \begin{bmatrix} L_2 \\ L_3 \end{bmatrix}_n \tag{99}$$

Taking the z-transform and collecting yields

$$\left[ (z - 1) - h \begin{bmatrix} 0 & -k \\ k & 0 \end{bmatrix} \right] \begin{bmatrix} L_1(z) \\ L_2(z) \end{bmatrix} = 0 \tag{100}$$

which has a nontrivial solution if

$$\left| (z - 1) - h \begin{bmatrix} 0 & -k \\ k & 0 \end{bmatrix} \right| = 0 \tag{101}$$

The characteristic equation of equation (100) is

$$(z - 1)^2 + h^2 k^2 = 0 \tag{102}$$

Equation (102) can be factored into two roots by inspection; the roots are

$$z = 1 \pm ihk \tag{103}$$

from which the solution to equations (99) by using approximation (35) is

$$\begin{bmatrix} L_2 \\ \\ L_3 \end{bmatrix} = e^{\frac{hk^2}{2}t}\left[\bar{c}_1 e^{i\left(k - \frac{h^2k^3}{3}t\right)} + \bar{c}_2\bar{e}^{-i\left(k - \frac{h^2k^3}{3}\right)t}\right] \tag{104}$$

where $\bar{c}_1$ and $\bar{c}_2$ are constant vectors. By using equations (104), the solution to equation (87) is

$$N = L_{1,o}^{\ 2} + e^{hk^2t}\left[L_{2,o}^{\ 2} + L_{3,o}^{\ 2}\right] \tag{105}$$

Note that for the case of cylindrical symmetry, the rate equations are linear (see eqs. (98)). For this case an expression can be found for the error when Adams-Bashforth second-order integration is used. Consider

$$\begin{bmatrix} L_2 \\ \\ L_3 \end{bmatrix}_{n+2} - \begin{bmatrix} L_2 \\ \\ L_3 \end{bmatrix}_{n+1} = \frac{h}{2}\left(3\begin{bmatrix} 0 & -k \\ \\ k & 0 \end{bmatrix}\begin{bmatrix} L_2 \\ \\ L_3 \end{bmatrix}_{n+1} - \begin{bmatrix} 0 & -k \\ \\ k & 0 \end{bmatrix}\begin{bmatrix} L_2 \\ \\ L_3 \end{bmatrix}_{n}\right) \tag{106}$$

Taking the z-transform and collecting terms yields

$$\left(z(z-1) - \frac{h}{2}(3z-1)\begin{bmatrix} 0 & -k \\ \\ k & 0 \end{bmatrix}\right)\begin{bmatrix} L_2(z) \\ \\ L_3(z) \end{bmatrix} = 0 \tag{107}$$

for which the characteristic equation is

$$z^2(z - 1)^2 + \frac{h^2k^2}{4}(3z - 1)^2 = 0 \tag{108}$$

which can be factored as

$$z(z - 1) = \pm i \frac{hk}{2}(3z - 1) \tag{109}$$

The roots of this equation are known to be

$$z_{1,2} \approx 1 - 2c^2 - 2c^4 \pm i\left(2c + 2c^3\right) \tag{110}$$

$$z_{3,4} \approx 2c^2 + 2c^4 \pm i\left(c - 2c^3\right) \tag{111}$$

where $c = \frac{hk}{2}$. (Compare eqs. (57) and (58).) The roots given by equation (111) are heavily damped and need not be considered. The solution obtained by using approximation (35) is

$$\begin{bmatrix} L_2 \\ \\ \\ L_3 \end{bmatrix} \approx e^{4\frac{h^3k^4}{16}t} \left( \bar{c}_1 e^{i\left(k + \frac{5}{12}h^2k^3\right)t} + \bar{c}_2 e^{-i\left(k + \frac{5}{12}h^2k^3\right)t} \right) \tag{112}$$

where $\bar{c}_1$ and $\bar{c}_2$ are the same as in equations (104). The solution to equation (88) is given as

$$N = L_{1,o}{}^2 + \left(L_{2,o}{}^2 + L_{3,o}{}^2\right) e^{8\frac{h^3k^4}{16}t} \tag{113}$$

Near spherical symmetry: Consider region II of figure 10 where nonlinear effects cannot be neglected (that is, relation (97) is no longer valid). In the nonlinear region K is no longer large compared with $\delta I / I_{22}{}^2$; this condition implies that

$$\frac{\left|I_{22} - I_{11}\right|}{I_{11}} \approx \frac{\left|I_{33} - I_{22}\right|}{I_{22}} \tag{114}$$

A solution to the general problem has not been found in region II. However, an approximate solution can be found for the Euler integration formula if, in addition to relation (114), the following relations also hold:

$$\left.\begin{aligned} \frac{|\delta I'|}{I_{11}^2} &\ll 1 \\ \frac{|\delta I|}{I_{22}^2} &\ll 1 \end{aligned}\right\} \tag{115}$$

where

$$\delta I' = I_{22} - I_{11} \tag{116}$$

$$\delta I = I_{33} - I_{22} \tag{117}$$

Relations (115) then define near spherical symmetry and equation (12) can be rewritten as

$$\begin{bmatrix} p \\ q \\ r \end{bmatrix} = \frac{1}{I_{22}} \begin{bmatrix} L_1 \\ L_2 \\ L_3 \end{bmatrix} + \begin{bmatrix} \frac{\delta I'}{I_{22}^2} & 0 & 0 \\ 0 & 0 & 0 \\ 0 & 0 & \frac{\delta I}{I_{22}^2} \end{bmatrix} \begin{bmatrix} L_1 \\ L_2 \\ L_2 \end{bmatrix} + O\left(\frac{\delta I^2}{I_{22}^3}\right) \tag{118}$$

Substituting equations (118) into equation (87) and neglecting terms in $\delta I$ and $\delta I'$ results in

$$\Delta N_n \approx \frac{h^2 N_n^2}{I_{22}^2} \sin^2 \chi_n \tag{119}$$

Dividing equation (119) by $N_n^2$ and letting

$$\kappa_n = \frac{h^2}{I_{22}^2} \sin^2 \chi_n \tag{120}$$

yields

$$\frac{\Delta N_n}{N_n^2} = \kappa_n \tag{121}$$

For $\Delta N_n << N_n$, equation (121) can be approximated by a perfect difference, namely,

$$\Delta\left(\frac{1}{N_n}\right) = \frac{\Delta N_n}{N_n N_{n+1}} \approx \frac{\Delta N_n}{N_n^2} \tag{122}$$

The approximate solution to equation (88) for nearly spherically symmetric vehicles when approximation (122) is valid is

$$N_n \approx \frac{N_o}{1 - N_o \sum_{j=0}^{n} \kappa_j} \tag{123}$$

which for $\kappa_j$ nearly constant or constant

$$N(t) \approx \frac{N_o}{1 - \frac{N_o \kappa}{h} t} \tag{124}$$

and the resulting error in the total angular momentum squared is

$$\epsilon(t) \approx \frac{N - N_o}{N_o} = \frac{N_o \kappa t}{h - N_o \kappa t} \tag{125}$$

Thrusted case: To study the on-off thrust controlled vehicle, assume that $\overline{M}$ is defined only on the integration intervals. This assumption neglects the small delays in applying thrust. The effects of this delay can be evaluated by analysis or by comparing solutions at two different interval sizes. The latter method was chosen since the fine detail of the limit cycle motion was not of great interest in this problem. Under this assumption, the $\overline{M}$ of equation (11) can be integrated exactly by using Euler integration.

By using Euler integration, the per-step change in the total angular momentum squared is

$$\Delta N_n = h\dot{N}_n + h^2\left(\omega_n^2 N_n \sin^2\chi_n + 2\omega_n N_n^{1/2} M_n \sin\chi_n \cos\gamma_n + M_n^2\right) \tag{126}$$

where $M$ is the magnitude of $\overline{M}$ and $\gamma$ is the angle between the $\dot{\overline{L}}$ and $\overline{M}$. Nominally, the control moment $\overline{M}$ is applied to $\overline{\omega}$. Since $\dot{\overline{L}}$ and $\overline{\omega}$ are orthogonal, $\gamma$ is always near $\pi/2$. Hence,

$$\Delta N_n \approx h\dot{N}_n + h^2\left(\omega_n{}^2 N_n \sin^2\chi_n + M_n{}^2\right) \tag{127}$$

From equation (127), the per-step deviation from Euler integration is

$$\Delta\epsilon_n \approx h^2\left(\omega_n{}^2 N_n \sin^2\chi_n + M_n{}^2\right) \tag{128}$$

The importance of this result is that the per-step error given by equation (127) is independent of the frequency associated with $\overline{M}$; only the magnitude $M$ contributes to the solution error.

It would seem that an impasse has been met since on-off control thrust dictates the use of Euler integration. However, equation (125) indicates rather poor behavior of the nonthrusted portion of the moment equations for this scheme. Equation (11) can be partitioned so that each term can be integrated in a manner most likely to yield a quality solution. To do this, consider the integral of equation (11).

$$\overline{L} = \int\left(\Omega \cdot \overline{L}\right)dt + \int\overline{M}\,dt \tag{129}$$

Define the partitioning as

$$\left.\begin{aligned} \overline{L}_1 &= \int\left(\Omega \cdot \overline{L}\right)dt \\ \overline{L}_2 &= \int\overline{M}\,dt \\ \overline{L} &= \overline{L}_1 + \overline{L}_2 \end{aligned}\right\} \tag{130}$$

The two terms, $\overline{L}_1$ and $\overline{L}_2$, can be integrated by using the Adams-Bashforth second-order and Euler integration schemes, respectively, and a high quality solution is obtained with little added complication.

Discussion of experiment.- The angular momentum rate equations were first analyzed for the nonthrusted case (that is, $\overline{M} = 0$) for two integration schemes. The analysis was done for two classes of vehicles which were nearly cylindrically symmetric and nearly spherically symmetric. The forms of the angular momentum rate equations are the same as those of the direction cosine rate equations with the exception of the nonlinearity defined by $\overline{\omega}$ as a function of the $\overline{L}$. For the near cylindrical case, the

equations are nearly linear and the solution for Euler and Adams-Bashforth second-order integration can be approximated.

The angular momentum rate equations were solved for initial conditions of

$$p = q = r = \frac{1}{\sqrt{3}} \frac{\text{radians}}{\text{sec}}$$

$$I_{11} = 500.0 \text{ kg-m}^2$$

$$I_{22} = 878.9 \text{ kg-m}^2$$

$$I_{33} = 881.9 \text{ kg-m}^2$$

$$h = \frac{1}{32} \text{ sec}$$

with Euler and Adams-Bashforth second-order integration schemes. For these values of inertias, the motion is described by the near cylindrical approximation. The predicted and computed motion for Euler integration is shown in figure 11 and the agreement is good. The corresponding predicted and computed errors for Adams-Bashforth second-order integration is shown in figure 12. Two computed errors are shown in figure 12; they are for $N_b = 27$ bits and $N_b = 48$ bits. The roundoff error is shown to be dominant on the 27 significant bit machine. The solution using extra precision is closely approximated by the approximate analytic solution of the Adams-Bashforth second-order integration. It is not clear at this time whether the roundoff error is caused from the induced error or the inherent error. The Adams-Bashforth scheme is sufficient for solving the nonthrusted portion of the angular momentum equations, the accuracy exceeding that of Euler integration by several orders of magnitude, even for $N_b = 27$ bits.

The use of Euler integration for a vehicle of near spherical symmetry is, in general, inadequate. The behavior of the total angular momentum squared was found not to be a positive definite form under Adams-Bashforth second-order integration. In general, one can expect the error due to Adams-Bashforth integration to be of several orders of magnitude less than that due to Euler integration.

It was assumed that the small time delays in applying thrust were negligible. This assumption clearly depends on the control system parameters. For the Gemini problem, the effects of these time delays were determined by comparing two solutions of different interval sizes which were $h = 31.25$ milliseconds and $h = 15.625$ milliseconds. The control system was placed in attitude hold and three stick deflections were commanded as follows:

(1) Roll right at one-half maximum rate for $0 \leqq t \leqq 3$ seconds

(2) Pitch up at one-half maximum rate for $10 \leqq t \leqq 13$ seconds

(3) Yaw right at one-half maximum rate for $20 \leqq t \leqq 23$ seconds

The results of these attitude-control cases are shown in figures 13 to 15. As seen from the figures, the gross behavior is, for all purposes, identical. There are small apparent discrepancies in the limit cycle and end point motion. Even so, these solutions show good agreement.

When $\overline{L}$ and $\overline{\omega}$ are parallel, the integration of the nonthrusted portion is integration-scheme independent. The $\overline{L}$ and $\overline{\omega}$ are parallel whenever the $\overline{\omega}$ (hence, the $\overline{L}$) lies along a principal axis. Most vehicles are constructed so that the body axis and principal axis are nearly alined. The typical pilot uses the single-axis technique (that is, a sequence of maneuvers about a single body axis at a time) for which $\overline{\omega}$ and $\overline{L}$ are nearly parallel. The primary contribution to the angular momentum is thrust which can be integrated exactly.

When either the $\overline{L}$ and $\overline{\omega}$ are nearly parallel and/or the magnitude of $\overline{\omega}$ is small, the roundoff error is the dominant error. Clearly, the most likely area of difficulty is in the limit cycle motion. The results indicate no serious instability in the limit cycle motion; thus, the only remaining question is the fuel usage in the limit cycle. The change in fuel usage will not be greatly affected for short-period flights; however, for full mission simulators where the motion is in the limit cycle for several hours, consideration should be given to the fuel cost due to computation errors.

In simulating the angular momentum rate equations on analog computers, the minimum pulse width of the attitude control moments is determined by the switching time of the computers logic components unless otherwise provided. An analogous situation occurs in digital simulation where the minimum pulse width (Euler integration) is the integration interval size unless it is provided by other means. In digital simulation problems where rather large integration intervals are used, a minimum pulse width must be provided. Large erroneous expenditures of fuel due to erratic limit cycle motion can be caused by oversized minimum pulse widths which are determined by the integration interval. Although the simulation of minimum pulse width on general purpose analog computers is somewhat difficult, this provision is an inherent consequence of digital simulation and requires only a small amount of simple logic.

It is often desired to compute the mass change of the simulated vehicle. The mass rate is usually given as proportional to thrust. Hence, Euler integration gives an exact representation of the mass since mass is a linear function of time or a constant.

## Translational Dynamics

Analytical development.- The mathematical model representing the trajectory motions is extremely nonlinear and therefore does not lend itself very readily to the type of analytical investigation made in the other sections. However, since the trajectory of the two vehicles referenced to inertial space is very smooth, some comments concerning truncation compared with roundoff effects can be made. The frequencies associated with the trajectories are on the order of $1.2 \times 10^{-3}$ radian/second. When this frequency is coupled with the maximum interval size, $h \approx 0.05$ second, the graph in figure 2 provides an estimate of the local truncation and roundoff errors (for $h\omega \leqq 6 \times 10^{-5}$ radian):

$$\epsilon_{tr} \approx 6 \times 10^{-10}$$

$$\epsilon_{r} \approx 6.2 \times 10^{-5}$$

The indication given by these results is that roundoff error constitutes most of the error in the solution of the trajectory motion. In order to verify the prime source of error and to evaluate the effects of the propagated truncation and roundoff errors, computer solutions with widely varying interval sizes can be compared with a double-precision fourth-order Runge-Kutta solution (or any other reliable solution).

Discussion of experiment.- The global errors, using double-precision fourth-order Runge-Kutta as a standard, in the trajectory variables (eqs. (A1) to (A16)) are shown in figure 16 as functions of the integration interval size at $t = 5004$ seconds. It is noted in figure 16 that the minimum global errors occur around an interval size of $h \approx 0.1$ second. However, because of the pilot input and the need for a smooth visual display, an upper bound on the interval size must be placed at 0.05 second (that is, $h \lessapprox 0.05$ sec). The logical choice, if constrained to powers of two to minimize roundoff effects, is $h = 2^{-5}$ second. Also, note that there is little difference in the global errors of Euler and Adams-Bashforth second-order integration; thus, truncation error constitutes a minor part of the total error and hence, contributes to the confirmation of the validity of error dominance. In figure 17 is the global error in two coordinates as a function of time for $h = 2^{-5}$ second. Again, it is apparent that roundoff error is by far the largest contributing error.

Further evidence verifying roundoff error (in particular, the induced error) as the major contributor to the global error is seen from the results in table II. There is excellent agreement between the standard solution and the partial double-precision (for control of induced error) second-order Adams-Bashforth solution. When compared with the single precision second-order Adams-Bashforth solution, the severity of the roundoff effects on a $N_b = 27$ bit class of machine is clearly indicated.

## TWO EXAMPLE PROBLEMS

In the past, the simulation engineer has relied heavily on an intuition developed from years of experience with analog (electronic differential analyzer) computation. The advent of digital simulation requires the building of a reliable intuition of the numerical processes of digital computation before digital simulation can become highly productive. It is for this reason that two example problems are considered.

The first problem is a Gemini-Agena rendezvous and station-keeping simulation. (See ref. 11.) This problem fits the class of problems studied in the analysis. Hence, the integration schemes discussed are directly applicable.

The second example is a modification of the first, the modification being the addition of an elastic tether (ref. 12) coupling the two vehicles' motion. The two vehicles are now somewhat like a single structure with internal degrees of freedom. Considered as a single vehicle, the system has a structural frequency that depends on the tether properties. The results of the analysis are no longer applicable in its entirety. However, these results are used as a starting point. The methods used to improve the digital program are discussed later.

Hopefully, several things will be accomplished in these two examples. FORTRAN is adequate in its present form for the IBM 7094-II, especially with regard to the amount of core and processing time for large simulation problems. The storage and processing time depend upon how well the FORTRAN compiler has been adapted to the particular machine being used. The integration schemes discussed in the analysis were not intended for blanket approval. The second example problem then gives the next logical step for arriving at a working simulation program. The tether program is a direct modification of the first. Hence, the effort involved to modify a large existing digital simulation program is better understood.

### Gemini-Agena Problem

Program development.- The physical problem being simulated was that of two vehicles in near-earth orbit. One of the vehicles was constrained to a planar orbit and was considered to be passive. Tumbling or any special orientation could be simulated with proper initial conditions on the inertial moment equations. No external thrust was provided. The other vehicle had a full six degrees of freedom. There were external thrust capabilities provided on this vehicle. The external thrust capabilities can be divided into two categories. The first category includes translational movement jets which were located approximately along each principal axes. These jets were used in a strict on-off fashion and were activated by the pilot's stick deflection. External thrust for the second-category attitude movements can be further subdivided into several modes

of operation. These jets could be activated by a system of switches and stick movements in either rate command with attitude hold, acceleration command, or pulse modes. Each of these modes was determined by using standard methods. A block diagram depicting the flow of the equations (eqs. (A4) to (A106)) is presented in figure 18. The control system was not listed in appendix A because of the difficulty of expressing the control system in equation form.

An exception has been made to the original Gemini-Agena problem. The "cage" mode of the Gemini control system has been deleted because of the present limited number of digital-analog converters but this deletion does not jeopardize the results of this study.

Discussion of experiment.- The Gemini-Agena station keeping and docking problem, the equations of which are discussed in appendix A, were programed for the IBM 7094-II in FORTRAN. This program was used with the Langley visual rendezvous simulator which is shown schematically in figure 3 of reference 12. Some of the results of this program are discussed in references 11 and 12. The integration schemes used in this program are given in the following table:

| Portion of program | Integration scheme used |
|---|---|
| Euler parameters | Adams-Bashforth second order |
| Control system | Adams-Bashforth second order |
| Angular momentum: | |
| Dynamic part | Adams-Bashforth second order |
| Thrust part | Euler |
| Trajectory: | |
| Dynamic part | Adams-Bashforth second order |
| Thrust part | Euler |
| Mass | Euler |

Subroutines such as sine, cosine, and square root provided with this language were used. This Gemini-Agena program was used in conjunction with a machine language program which provided mode control and communications with a real-time clock and simulation hardware. The integration interval used was $h = 31.25$ msec. The two programs combined required about 6000 locations in core and less than 4 msec for all calculations and input/output functions. This program leaves approximately 85 percent of core unused and the central processor free approximately 87 percent of the time.

The amount of core and central processing time required for this problem clearly indicates that more than one such problem could easily be processed simultaneously

(multiprocessing) with sufficient conversion equipment and a control program to provide independent mode control. (See ref. 3 for other discussions of multiprocessing.) This operation is limited in that a single program must contain all such problems to be compiled as a group. On a more sophisticated machine, it would be desirable to compile, process, and terminate a real-time simulation job while processing other real-time programs and/or nonreal-time programs whenever sufficient core or central processing time is available (multiprograming).

## Gemini-Agena Tether Problem

Program development.- The system considered is essentially a modification of the Gemini-Agena rendezvous and docking problem already considered. The equations of motion are referenced to the center of mass to retain a similar form for the translational equations except, of course, for the elastic coupling. A more complete discussion of this problem is in reference 12.

The longitudinal translational vibration frequency was estimated to be 0.5 Hertz for the worst case. The expected relative local truncation and roundoff error for this mode is ($\omega h \approx 9.6 \times 10^{-2}$ radian)

$$\epsilon_{tr} \approx 1.5 \times 10^{-4}$$

$$\epsilon_{r} \approx 3.8 \times 10^{-8}$$

for $h = 31.25$ msec where a second-order integration technique is assumed. The new equations of motion were programed and Adams-Bashforth second-order integration schemes were used for both the translational and rotational degrees of freedom. The program was initially checked by using this method of integration and the answers were compared with a fourth-order Runge-Kutta solution. The observed computation errors (Error = |Runge-Kutta – Adams-Bashforth|/maximum value) were on the order of or less than 10 percent.

At this point a simple analysis was made. The initial conditions can be chosen so that the longitudinal translational equation becomes

$$\ddot{x} = -\omega^2 x$$

where $\omega$ is related to the masses of the vehicles and spring constant of the tether. The roots using Adams-Bashforth second-order integration are found to be

$$z_{1,2} \approx 1 - 2c^2 - 2c^4 \pm i2c(1 + c^2)$$

$$z_{3,4} \approx 2c^2 + 2c^4 \pm ic(1 - 2c^2)$$

where $c = h\omega/2$.

Transforming these roots to the s-plane $\left(s = \frac{1}{h} \log_e z\right)$ and using approximation (35) yields

$$s_{1,2} \approx -\frac{3}{4} h^3\omega^4 \pm i\omega \left(1 + \frac{5}{8} h^2\omega^2\right)$$

with the real parts of $s_{3,4}$ large and negative.

The next scheme considered was to use Adams-Bashforth second-order scheme to obtain $\dot{x}$ and the Adams-Moulton second-order scheme to obtain $x$:

$$\dot{x}_{i+2} = \dot{x}_{i+1} + \frac{h}{2}\left(3\ddot{x}_{i+1} - \ddot{x}_i\right) = \dot{x}_{i+1} - \frac{h\omega^2}{2}\left(3x_{i+1} - x_i\right)$$

and

$$x_{i+2} = x_{i+1} + \frac{h}{2}\left(\dot{x}_{i+2} + \dot{x}_{i+1}\right)$$

which can be written in matrix form as

$$\begin{bmatrix} E(E - 1) & \frac{h\omega^2}{2}(3E - 1) \\ -\frac{h}{2} E(E + 1) & E(E - 1) \end{bmatrix} \begin{bmatrix} \dot{x}_i \\ x_i \end{bmatrix} = \begin{bmatrix} 0 \\ 0 \end{bmatrix}$$

If the z-transform ($E \rightarrow z$) is taken, the characteristic equation is

$$z\left[z(z - 1)^2 + c^2(z + 1)(3z - 1)\right] = 0$$

Hence, one root is zero and the factor in brackets can be written as

$$(z - c^2)\left[z^2 - 2(1 - 2c^2)z + 1\right] + 4zc^4 = 0$$

If the system is assumed to be nearly stable (that is, $|z| \lesssim 1$), the last term is

$$4zc^4 \approx 10^{-6}$$

and can be neglected because of its small value so that

$$(z - c^2)\left[z^2 - 2(1 - 2c^2)z + 1\right] \approx 0$$

Thus, the four roots are

$$z_{1,2} \approx (1 - 2c^2) \pm i2c\left(1 - \frac{1}{2}c^2\right)$$

$$z_3 = c^2$$

$$z_4 = 0$$

Transforming these roots into the s-plane yields

$$s_{1,2} \approx -\frac{3}{16}h^3\omega^4 \pm i\omega\left(1 + \frac{3}{8}h^2\omega^2\right)$$

where $s_3$ is large, real, and negative and $s_4 = -\infty$. Hence, the roots are by a factor of four closer to the real roots in damping and the frequency error has improved by almost a factor of two.

Discussion of experiment.- The Gemini-Agena program, discussed in the previous section, was modified to accommodate the tether and the additional degree of freedom. The integration schemes were not changed in the initial stages of checkout. The observed computation errors were on the order of or less than 10 percent when compared with an all-fourth-order Runge-Kutta solution. The Adams-Bashforth scheme was then modified by applying the Adams-Moulton second-order corrector once to all translational and rotational variables. The solution obtained from this integration scheme was within one-half percent of the fourth-order Runge-Kutta solution and the addition to the computation time is virtually undetectable. The final integration schemes used are summarized as follows:

| Portion of program | Integration scheme used |
|---|---|
| Euler parameters | Adams-Moulton predictor-corrector* |
| Control system | Adams-Bashforth second order |
| Angular momentum: | |
| Dynamic part | Adams-Moulton predictor-corrector* |
| Thrust part | Euler |
| Trajectory: | |
| Dynamic part | Adams-Moulton predictor-corrector* |
| Thrust part | Euler |
| Mass | Euler |

*Second order with corrector applied once.

The amount of core and central processor time required was virtually no different than that required for the Gemini-Agena problem. The modification and ensuing checkout process was accomplished in less than one man-day (8 hours). This time does not include the Runge-Kutta check case that was already available.

## RESULTS AND DISCUSSION

The basic equations considered in the analysis are common to most flight simulation problems. In particular coordinate transformations, the attitude control system and angular momentum equations commonly reoccur. The greatest variations are in the addition of aerodynamics, structural effects, and the description of the trajectory which could cause large deviations from the conclusions of this study. For example, the addition of nonlinear aerodynamic moments could greatly alter the basic stability of the angular momentum equations as discussed in the analysis. In some special applications, the trajectory is computed from the body-axis force equations which are of the form of the direction cosine rate equations, the constant of motion being the total velocity squared for no applied forces. The addition of body bending modes and the flutter of appendages generally raise the frequencies of the problem. The effects of truncation error must then be reexamined and a higher order integration scheme may need to be applied.

The trajectory calculations of many simulations, in general, exhibit a low-frequency component, where the frequency of this component is several orders of magnitude smaller than the frequencies associated with the remainder of the problem. Hence, roundoff error will generally be a concern. The analysis of roundoff and truncation error should be helpful in determining the need for concern. Hence, if a particular problem has the local relative roundoff and truncation error of the same order of magnitude, great care should be applied to determine the propagated roundoff error. If roundoff error is important, partial double precision should be applied to as few of the sensitive variables as possible to obtain a reasonable solution.

Roundoff error has been shown to be a prime consideration on a computer with a 27-bit fractional part. Langley Research Center now has available a complex of Control Data series 6000 computers. The fractional portion of the floating-point word is 48 bits in this computer series; hence, the roundoff error is reduced by $2^{-21}$ as compared with the error for the $N_b = 27$ bit machine used in this study.

Because of the roundoff error, the choice of integration interval size is greatly limited for manned simulations of this class of problems on an $N_b = 27$ bit computer (that is, 31.25 msec $\lessapprox h \leqq 50$ msec where the lower limit is chosen to control roundoff error). Greater flexibility is afforded on the 6000 series machines (namely, $2^{-21} \times 31.25$ msec $\approx 10^{-5}$ msec $\lessapprox h \leqq 50$ msec) without roundoff error becoming a serious problem.

## APPLICATIONS

Langley Research Center now has three Control Data series 6000 computers with multiprograming capability in a mixed real-time and/or nonreal-time environment. The prime computer for real-time jobs is a 6600 computer with a $131K)_{10}$ memory. Most of the problems solved digitally to this date are problems which are clearly too large or marginally large for the analog-TRICE computer complex (TRICE, a digital differential analyzer) at the Langley Research Center. There are several real-time simulation consoles which provide the simulation engineer program control, input, and output (to change problem parameters). The language used with this computer complex is the FORTRAN language with a relatively early compiler; the compiler is still relatively inefficient with regard to central processor time. A brief description of several flight simulation problems with corresponding vital statistics that have been completed or are currently in progress follows:

The lunar-orbit and landing-approach simulations were formulated for real-time digital operation. This problem consists of three separate vehicles each employing six degrees of freedom and relative geometry between vehicles. All integrations used second-order Adams-Bashforth and Euler integrations as previously discussed. The results were largely compared with analytic results and showed good agreement. The interval size was 1/64 second or 15.625 milliseconds (this size could be increased) which was chosen to accommodate the minimum impulse of the attitude-control system. The required central processor time was approximately 7 milliseconds including all overhead. The memory requirement was approximately $37K)_{10}$. $(37K)_{10}$ denotes 37 000 in decimals.)

An Apollo-LEM rendezvous program was obtained by modifying the lunar-orbit and landing-approach program. The integration schemes and interval size were the same. The central processor time was approximately 8.5 milliseconds with $24K)_{10}$ core locations required.

The lunar-orbit and landing-approach program was again modified for an Apollo-abort study. Among the features retained in this modification is staging capability. The central processor time was approximately 7 milliseconds and less than $24K)_{10}$ core locations were required.

The original Gemini-Agena program, the first example problem for the IBM 7094-II, was converted for the Control Data 6600 computer. The interval size was $2^{-5}$ second or 31.25 milliseconds when second-order Adams-Bashforth and Euler integrations were used. The central processor time was approximately 2 milliseconds with $6K)_{10}$ core locations required.

A simulation program of F-105 and F-86 fighter airplanes has been developed to study the feasibility of employing research simulators for evaluating the tactical effectiveness of fighter aircraft. In the program, each airplane had six degrees of freedom, relative geometry equations, and simplified line-of-sight scoring equations. Adams-Bashforth second-order integration was used exclusively with an interval size of $2^{-5}$ second or 31.25 milliseconds. The error was less than 0.5 percent when compared with fourth-order Runge-Kutta check cases. The total central processor time including input/output and the real-time monitor is approximately 17 milliseconds and requires less than $40K)_{10}$ core locations. (Note that this program includes two complete airplane simulations.)

The HL-10 lifting body was simulated in full six degrees of freedom using second-order Adams-Bashforth integration with an interval size of $2^{-5}$ second or 31.25 milliseconds. The errors were again under 0.5 percent. The total central processor time was 10.21 milliseconds with $16.5K)_{10}$ core locations required.

The static test program is a FORTRAN-coded simulation of an orbiting laboratory of an Apollo telescope mount (ATM) configuration. Six elastic-body modes are incorporated directly in the model, the other modes being accounted for in a quasi-static model. The program is being used to evaluate the use of a control-moment-gyroscope system to generate control torques for attitude stabilization of the telescope mount. This program runs in a closed loop with three control-moment gyroscope prototypes mounted on a moving-base simulator. The loop is closed through 14 bits plus the sign, analog-digital-conversion equipment which transmits the measured torque output of the control-moment-gyroscope system. There are provisions for external torque input from taped frequency-modulated analog or discrete crew motion disturbances. The fourth-order Runge-Kutta integration scheme is used with $h = 31.25$ milliseconds which is sufficient to keep errors below 0.2 percent when compared with a nonreal-time solution. The central processor time is about 19 msec with approximately $16K)_{10}$ core locations required.

In addition to these large simulation programs, many small simulation problems have been studied. Many advantages have become apparent from these small jobs. These jobs can be used to fill central processor time slots and core positions not used by the large simulation jobs (which is otherwise filled with background nonreal-time jobs). Many research engineers are familiar with the FORTRAN language; hence, the research engineer can prepare his own simulation program without relying on highly specialized personnel. It has been demonstrated that inexperienced personnel can operate even large digital simulation problems with little supervision.

## CONCLUDING REMARKS

The analysis indicates that the lower order integration schemes, second-order Adams-Bashforth and Euler, are generally adequate for the class of nonaerodynamic rigid-body problems. The accuracy of these techniques indicates that these integration schemes are reasonable starting points for similar flight simulations. In the event of failure, a simple analysis, similar to those contained in this paper, can often be performed to indicate the next step in determining a working simulation program. The Adams-Moulton second-order corrector is a reasonable second step. A relatively efficient computer program in either case is indicated by the computer results of this study.

The Green's function technique employed to solve the gyroscope equations is exact when the forcing function is linear over the integration interval. Higher order terms in the forcing function can be carried in this technique with effectively no added computer time. This method should be extended to include such effects as nonwindup limiting (piecewise linearity). This technique can also be extended to other linear and piecewise linear systems. For example, consideration should be given to the computation of structural effects where frequencies are often high.

Assuming the control moment to be defined only on the ends of the integration intervals and hence neglecting small time delays in applying thrust was shown to be valid for the Gemini-Agena example problems. This procedure was also valid for other vehicles. Clearly, this approximation is dependent on the control system parameters and further analytical work is needed. However, a simple check by changing the integration interval size should lend confidence in the solution of any particular problem.

Roundoff error was shown to be marginal on a floating-point machine with a 27-bit fractional part with an integration interval of 31.25 milliseconds. Partial double precision was shown to be an effective method for controlling the induced error. It is recommended that double precision be used with care because of the additional central processor time. On machines with a fractional part less than 27 bits, partial double precision is likely to be unavoidable. In any case, efforts should be made to control the inherent error and error dominance should be used on short word machines (less than 27-bit fractional part) to locate areas where the induced error is likely to cause difficulty.

Low-order multistep integration techniques were applied to two large simulation problems and solved on an IBM 7094-II (a large last-generation digital computer). The results of these experiments show these problems to be small compared with the capacity of this computer. Hence, multiprocessing (concurrent processing of more than one problem but in a dependent manner since all problems must be compiled as a single program) on the last-generation computer is a reasonable approach to reduce cost. Otherwise, a smaller slower machine (hence, less expensive) is sufficient for many simulation problems.

Recent computers with hardware and software oriented toward multiprograming in a real-time environment (concurrent processing and/or compiling more than one problem independently) are clearly indicated as desirable for a general-purpose simulation laboratory. Langley Research Center now has a complex of Control Data series 6000 computers with a multiprograming system. This mode of operation has proven to be very successful in that one or more large real-time simulation programs can be processed or compiled, with other smaller real-time or nonreal-time jobs giving better utilization of the computer's capabilities.

The use of FORTRAN as a simulation language is shown to be adequate, especially in view of the core storage and central processor time required for the several simulation problems discussed, most of which involved two or more vehicles. However, the efficiency of the FORTRAN language depends on how well the compiler has been adapted to the computer used. The efficiency of the object code of the 6600 computer used for this computation is not yet commensurate with the capabilities of this machine.

This investigation has given primary consideration to the simulation of nonaerodynamic vehicles. The conservative attitude about possible instability when aerodynamic control is added to the simulation is largely unwarranted. Two rather unconventional aircraft simulations, the F-105 airplane and the HL-10 lifting body, indicate that the integration schemes are applicable to a wide class of aerodynamic problems.

Langley Research Center,
National Aeronautics and Space Administration,
Langley Station, Hampton, Va., August 21, 1968,
125-23-03-02-23.

# APPENDIX A

## GEMINI-AGENA EQUATIONS OF MOTION

By Roland L. Bowles
Langley Research Center

The purpose of this appendix is to present in concise format, with no derivation, the basic equations used in this study. The following equations have been developed to simulate the Gemini-Agena configuration in eleven degrees of freedom. These equations are particularly well suited for simulation of terminal rendezvous and such close-in operations as station-keeping and fly-around missions. Foremost in the selection of this formulation was that it meet mission and simulation hardware (visual docking simulator) requirements and overcome computing difficulties with this class of piloted simulations.

### Equations of Motion

The force equations defining relative motion of the observer vehicle (three degrees of freedom) are referred to a rotating local vertical axis system centered in the target vehicle (two degrees of freedom). Polar coordinates $(r_S, \theta_S)$ are employed to locate the center of gravity of the nonthrusted target vehicle with respect to inertial space. There is essentially no restriction imposed on the eccentricity of the target orbits. Basic coordinate systems and relative geometry of the two vehicles are shown in figure 1. Both vehicles are assumed to be moving over a homogeneous nonrotating spherical earth.

In order to improve absolute computational accuracy and increase effective computer resolution, perturbated equations were used to generate the target orbit. For target orbits of moderate eccentricity, there are obvious computational advantages to be gained by transforming the dependent variables to represent deviations from a nominal circular orbit. In this manner the importance of computer errors for orbital or near-orbital simulations can be minimized. The necessary dependent variable transformations are

$$\rho = \frac{r_S}{r_O} - 1 \tag{A1}$$

$$\left.\begin{aligned} \delta &= \frac{V}{V_O} - 1 \\ V_O &= \sqrt{g_O r_O} \end{aligned}\right\} \tag{A2}$$

where $r_o$ is the radius of the reference orbit, $g_o$ is gravity acceleration at $r_s = r_o$, and $V_o$ is the characteristic velocity of a vehicle in a circular orbit at radial distance $r_o$. In equation (A2), V is defined as the tangential velocity at any time (that is, $V = -r_s\dot{\theta}_s$). For computer scaling purposes, it is advantageous to choose $r_o$ equal to the mean radius of the highest apogee and lowest perigee trajectories which must be computed. Hence,

$$r_o = r_e + \frac{h_a + h_p}{2} \tag{A3}$$

where $r_e$ is the earth radius and $h_a$ and $h_p$ are the apogee and perigee altitudes, respectively. Thus, the nondimensional perturbation variable $\rho$ will have a symmetric excursion about $\rho = 0$, over one orbital period. The degree of symmetry for $\delta$ depends strongly on the eccentricity of the orbit to be generated. By using the definitions of $\delta$ and $\rho$ in addition to the well-known Keplarian equations of motion for two-dimensional orbits and by making use of the fact that the orbital angular momentum is a constant of the motion, the resulting perturbation equations can be written as

$$\frac{1}{\omega_o{}^2}\ddot{\rho} = \frac{K_o{}^2 + 2K_o - \rho}{(1 + \rho)^3} \tag{A4}$$

$$\dot{\theta}_s = -\omega_o\left[\frac{1 + K_o}{(1 + \rho)^2}\right] \tag{A5}$$

where $\omega_o{}^2 = \frac{g_o}{r_o}$ and $K_o$ is specified from initial conditions (that is, $K_o = \delta(0)\left[1 + \rho(0)\right] + \rho(0)$). The coordinates $(r_s, \theta_s)$ are computed as follows:

$$r_s = r_o(1 + \rho) \tag{A6}$$

$$\theta_s = \theta_s(0) + \int_0^t \dot{\theta}_s \, d\tau \tag{A7}$$

Equations (A4) and (A5) are characterized by divisions which have a denominator of the form $(1 + \rho)^n$ where $n$ is an integer and typically $\rho << 1$.

The observer vehicle is located relative to the target local vertical by the three components of $\overline{R}$ that is, $(\overline{R} = x,y,z)$. Since $|\overline{R}| << r_s$ for missions considered in this simulation, the solution can be considerably enhanced by expanding the gravity gradient which appears in the equation for $\ddot{\overline{R}}$ and by retaining terms to the desired order of accuracy. Relative equations which are correct to the second order in the

gravity gradient were utilized in this study. The scalar equations used to define relative motion of the observer vehicle are

$$\ddot{x} + 2\dot{\theta}_S\dot{z} + \ddot{\theta}_S z - \frac{x}{1+\rho}\left[\ddot{\rho} - \frac{3\omega_o{}^2}{r_o}\frac{z}{(1+\rho)^3}\right] = \frac{T_X}{m} \tag{A8}$$

$$\ddot{z} - 2\dot{\theta}_S\dot{x} - \ddot{\theta}_S x - z\dot{\theta}_S{}^2 - \frac{2\omega_o{}^2 z}{(1+\rho)^3} + \frac{3}{2}\frac{\omega_o{}^2}{r_o}\frac{1}{(1+\rho)^4}\left(x^2 + y^2 - 2z^2\right) = \frac{T_Z}{m} \tag{A9}$$

$$\ddot{y} + \frac{\omega_o{}^2}{(1+\rho)^3}y + \frac{3\omega_o{}^2}{r_o}\frac{yz}{(1+\rho)^4} = \frac{T_Y}{m} \tag{A10}$$

where $T_X$, $T_Y$, and $T_Z$, are components of observer vehicle control forces resolved in the target local vertical axis system, and $m$ designates the constant mass of the observer vehicle. Acceleration coupling terms $\ddot{\theta}_S$ and $\ddot{\rho}$ resulting from elliptical target motion are retained. The variables $\dot{\theta}_S$, $\ddot{\theta}_S$, $\ddot{\rho}$, and $\rho$ are found from equations (A4) and (A5).

Components of observer-vehicle thrust forces resolved in the target local vertical (that is, $T_X$, $T_Y$, and $T_Z$) are defined as

$$T_X = a_{11}T_{X,b} + a_{12}T_{Y,b} + a_{13}T_{Z,b} \tag{A11}$$

$$T_Y = a_{21}T_{X,b} + a_{22}T_{Y,b} + a_{23}T_{Z,b} \tag{A12}$$

$$T_Z = a_{31}T_{X,b} + a_{32}T_{Y,b} + a_{33}T_{Z,b} \tag{A13}$$

where $T_{X,b}$, $T_{Y,b}$, and $T_{Z,b}$ are body-axis force summations and $a_{ij}$ are direction cosines relating the observer vehicle body axes to the target local vertical. The body-force summation, for the Gemini thruster configuration, can be written as

$$T_{X,b} = T_{X+}K_1 + T_{X-}K_2 + \left(T_{Y+} + T_{Y-} + T_{Z+} + T_{Z-}\right)K_3 \tag{A14}$$

$$T_{Y,b} = \left(T_{Y+} - T_{Y-}\right)K_4 + T_{\psi-} - T_{\psi+} \tag{A15}$$

$$T_{Z,b} = \left(T_{Z+} - T_{Z-}\right)K_2 + \left(T_{Y-} - T_{Y+}\right)K_5 + T_{\theta+} - T_{\theta-} \tag{A16}$$

where $T_{X\pm}$, $T_{Y\pm}$, $T_{Z\pm}$, $T_{\psi\pm}$, and $T_{\theta\pm}$ are "on-off" signals of appropriate magnitude, and the constants $K_j$ are defined as

$$K_1 = \cos 7.6^o$$

$$K_2 = \cos 26^o$$

$$K_3 = \sin 26^o$$

$$K_4 = \cos 26^o \cos 5^o$$

$$K_5 = \cos 26^o \sin 5^o$$

No provision has been made for simulating individual jet failures. The direction cosines $a_{ij}$ are computed as follows:

$$a_{11} = b_{11} \sin \theta_s + b_{13} \cos \theta_s \tag{A17}$$

$$a_{12} = b_{21} \sin \theta_s + b_{23} \cos \theta_s \tag{A18}$$

$$a_{13} = b_{31} \sin \theta_s + b_{33} \cos \theta_s \tag{A19}$$

$$a_{31} = -b_{11} \cos \theta_s + b_{13} \sin \theta_s \tag{A20}$$

$$a_{32} = -b_{21} \cos \theta_s + b_{23} \sin \theta_s \tag{A21}$$

$$a_{33} = -b_{31} \cos \theta_s + b_{33} \sin \theta_s \tag{A22}$$

$$a_{21} = b_{12} \tag{A23}$$

$$a_{22} = b_{22} \tag{A24}$$

$$a_{23} = b_{32} \tag{A25}$$

where $\theta_s$ has been defined previously (fig. 11) and $b_{ij}$ are direction cosines relating the observer vehicle body axes to inertial space. The $b_{ij}$ elements, specified as a function of four parameters (quaternion elements), are written as

$$b_{11} = 2\left(a^2 + d^2\right) - 1 \tag{A26}$$

$$b_{12} = 2(ab - cd) \tag{A27}$$

$$b_{13} = 2(ac + db) \tag{A28}$$

$$b_{21} = 2(ab + cd) \tag{A29}$$

$$b_{22} = 2\left(b^2 + d^2\right) - 1 \tag{A30}$$

$$b_{23} = 2(cb - ad) \tag{A31}$$

$$b_{31} = 2(ac - bd) \tag{A32}$$

$$b_{32} = 2(cb + ad) \tag{A33}$$

$$b_{33} = 2\left(c^2 + d^2\right) - 1 \tag{A34}$$

The parameters a, b, c, and d are bounded continuous functions of time and can be generated by knowing the components of the observer vehicle inertial angular velocity resolved in the body axes. The x, y, and z angular velocity components are defined as p, q, and r, respectively. Expressed in terms of p, q, and r, the differential equations defining the rotation parameters are

$$\dot{a} = \frac{1}{2}\left(-pd - qc + rb\right) - K_\epsilon a\epsilon \tag{A35}$$

$$\dot{b} = \frac{1}{2}\left(pc - qd - ra\right) - K_\epsilon b\epsilon \tag{A36}$$

$$\dot{c} = \frac{1}{2}\left(-pb + qa - rd\right) - K_\epsilon c\epsilon \tag{A37}$$

$$\dot{d} = \frac{1}{2}\left(pa + qb + rc\right) - K_\epsilon d\epsilon \tag{A38}$$

where $\epsilon$ is defined as

$$\epsilon = a^2 + b^2 + c^2 + d^2 - 1 \tag{A39}$$

and $K_\epsilon$ is a gain constant which is determined empirically on the computer.

## APPENDIX A

The angular momentum vector is related to the angular velocity by a linear transformation. By using this basic definition, the body angular rates are computed as follows:

$$p = I_{11}'L_1 + I_{12}\,L_2 + I_{13}'L_3 \tag{A40}$$

$$q = I_{21}'L_1 + I_{22}'L_2 + I_{23}'L_3 \tag{A41}$$

$$r = I_{31}'L_1 + I_{32}'L_2 + I_{33}'L_3 \tag{A42}$$

where $I_{ij}'$ are the elements of the inverse inertia matrix, and by definition, $I_{ij}' = I_{ji}'$ (symmetric matrix).

The components of angular momentum $L_1$, $L_2$, and $L_3$ can be generated as a function of time by knowing the external moments acting on the observer vehicle. The differential equations defining the angular momentum components are

$$\dot{L}_1 = rL_2 - qL_3 + M_1 \tag{A43}$$

$$\dot{L}_2 = pL_3 - rL_1 + M_2 \tag{A44}$$

$$\dot{L}_3 = qL_1 - pL_2 + M_3 \tag{A45}$$

where $M_1$, $M_2$, and $M_3$ are external moment summations resulting from attitude jets located on the observer vehicle. The moments are computed from the following equations

$$\begin{aligned} M_1 = {} & \left[(M_1)_{T_{\psi+}} - (M_1)_{T_{\psi-}}\right] + \left[(M_1)_{T_{\theta-}} - (M_1)_{T_{\theta+}}\right] + \left[(M_1)_{T_{\phi+}} - (M_1)_{T_{\phi-}}\right] \\ & + \left[(M_1)_{T_{x+}} + (M_1)_{T_{x-}}\right] + \left[(M_1)_{T_{y+}} - (M_1)_{T_{y-}}\right] + \left[(M_1)_{T_{z+}} - (M_1)_{T_{z-}}\right] \end{aligned} \tag{A46}$$

$$\begin{aligned} M_2 = {} & \left[(M_2)_{T_{\theta+}} - (M_2)_{T_{\theta-}}\right] + \left[(M_2)_{T_{x-}} - (M_2)_{T_{x+}}\right] - \left[(M_2)_{T_{y+}} + (M_2)_{T_{y-}}\right] \\ & + \left[(M_2)_{T_{z-}} - (M_2)_{T_{z+}}\right] \end{aligned} \tag{A47}$$

$$\begin{aligned} M_3 = {} & \left[(M_3)_{T_{\psi+}} - (M_3)_{T_{\psi-}}\right] + \left[(M_3)_{T_{x-}} - (M_3)_{T_{x+}}\right] + \left[(M_3)_{T_{y+}} - (M_3)_{T_{y-}}\right] \\ & - \left[(M_3)_{T_{z+}} + (M_3)_{T_{z-}}\right] \end{aligned} \tag{A48}$$

Standard convention has been adopted for positive yaw, pitch, and roll.

## APPENDIX A

The Agena target vehicle is assumed to be passive; however, tumbling capability in three degrees of freedom was simulated. The equations defining the target rotational motion are identical in form to those previously given for the observer vehicle, with the exception $M_1 = M_2 = M_3 = 0$. The necessary equations are summarized below:

The transformations relating target body axes to inertial space are

$$b_{11}' = 2\left(e^2 + f^2\right) - 1 \tag{A49}$$

$$b_{12}' = 2(eg - hf) \tag{A50}$$

$$b_{13}' = 2(eh + fg) \tag{A51}$$

$$b_{21}' = 2(eg + hf) \tag{A52}$$

$$b_{22}' = 2\left(g^2 + f^2\right) - 1 \tag{A53}$$

$$b_{23}' = 2(hg - ef) \tag{A54}$$

$$b_{31}' = 2(eh - gf) \tag{A55}$$

$$b_{32}' = 2(hg + ef) \tag{A56}$$

$$b_{33}' = 2\left(h^2 + f^2\right) - 1 \tag{A57}$$

The rotation parameters e, f, g, and h are computed from

$$\dot{e} = \frac{1}{2}\left(-p_t f - q_t h + r_t g\right) - K_\epsilon e \epsilon_t \tag{A58}$$

$$\dot{g} = \frac{1}{2}\left(p_t h - q_t f - r_t e\right) - K_\epsilon g \epsilon_t \tag{A59}$$

$$\dot{h} = \frac{1}{2}\left(-p_t g + q_t e - r_t f\right) - K_\epsilon h \epsilon_t \tag{A60}$$

$$\dot{f} = \frac{1}{2}\left(p_t e + q_t g + r_t h\right) - K_\epsilon f \epsilon_t \tag{A61}$$

where $\epsilon_t = e^2 + g^2 + h^2 + f^2 - 1$ and $K_\epsilon$ is constant. The target vehicle body rates are given as

$$p_t = J_{11}'H_1 + J_{12}'H_2 + J_{13}'H_3 \tag{A62}$$

$$q_t = J_{21}'H_1 + J_{22}'H_2 + J_{23}'H_3 \tag{A63}$$

$$r_t = J_{31}'H_1 + J_{32}'H_2 + J_{33}'H_3 \tag{A64}$$

where $J_{ij}'$ are elements of the inverse inertia matrix, and $H_j$ are components of the target vehicle angular momenta. The angular momentum components are computed as follows:

$$\dot{H}_1 = r_t H_2 - q_t H_3 \tag{A65}$$

$$\dot{H}_2 = p_t H_3 - r_t H_1 \tag{A66}$$

$$\dot{H}_3 = q_t H_1 - p_t H_2 \tag{A67}$$

Simulation Hardware Equations

This section is primarily devoted to the geometric relationships existing between the target image and the pilot's line of sight. The vector represented by the directed line segment from the pilot's eye to the center of gravity of the target vehicle defines the space line of sight (los). The components of the vector $\overline{R} = -x,-y,-z$ resolved in the observer vehicle body axes are given as

$$R_{X,o} = -\left(a_{11}x + a_{21}y + a_{31}z\right) \tag{A68}$$

$$R_{Y,o} = -\left(a_{12}x + a_{22}y + a_{32}z\right) \tag{A69}$$

$$R_{Z,o} = -\left(a_{13}x + a_{23}y + a_{33}z\right) \tag{A70}$$

Combining equations (A68) to (A70) with the pilot's eye offsets yields

$$\Delta x = R_{X,o} - x_p \tag{A71}$$

$$\Delta y = R_{Y,o} - y_p \tag{A72}$$

$$\Delta z = R_{Z,o} - z_p \tag{A73}$$

## APPENDIX A

The angles $\alpha$ and $\beta$ which specify the direction of the line of sight (los) with respect to the observer are defined as for mirror drives as

$$\alpha = \tan^{-1} \frac{\Delta y}{\Delta x} \tag{A74}$$

$$\beta = \tan^{-1} \frac{-\Delta z}{\left[(\Delta x)^2 + (\Delta y)^2\right]^{1/2}} \tag{A75}$$

The relative range $\left(\text{that is, } \left|\overline{R}_{los}\right|\right)$ which is used to drive the range bed is computed as follows:

$$\left|\overline{R}_{los}\right| = + \left[(\Delta x)^2 + (\Delta y)^2 + (\Delta z)^2\right]^{1/2} \tag{A76}$$

The direction cosines relating the target body axes to the line-of-sight axis system are now determined. This transformation is represented by the matrix $D = \left[\phi_R\right]_{los} \left[\mu\right]_Y \left[\nu\right]_Z$, which is obtained by applying three successive simple rotations about the specified axes. Alternately, the matrix $D$ can be expressed in terms of known information; that is,

$$D = \left[\beta\right]_Y \left[\alpha\right]_Z BB'^T \tag{A77}$$

where $\left[\alpha\right]_Z$ and $\left[\beta\right]_Y$ are simple rotations about the Z-observer body axis and the new Y-axis, respectively, and the matrices $B$ and $B'^T$ are defined by the matrix elements given by equations (A26) to (A34) and equations (A49) to (A57). The superscript $T$ denotes the matrix transpose operation. Expanding equation (A77) yields

$$d_{11} = f_{11} \cos\alpha \cos\beta + f_{21} \sin\alpha \cos\beta - f_{31} \sin\beta \tag{A78}$$

$$d_{12} = f_{12} \cos\alpha \cos\beta + f_{22} \sin\alpha \cos\beta - f_{32} \sin\beta \tag{A79}$$

$$d_{13} = f_{13} \cos\alpha \cos\beta + f_{23} \sin\alpha \cos\beta - f_{33} \sin\beta \tag{A80}$$

$$d_{21} = -f_{11} \sin\alpha + f_{21} \cos\alpha \tag{A81}$$

$$d_{22} = -f_{12} \sin\alpha + f_{22} \cos\alpha \tag{A82}$$

$$d_{23} = -f_{13} \sin\alpha + f_{23} \cos\alpha \tag{A83}$$

$$d_{31} = f_{11} \cos \alpha \sin \beta + f_{21} \sin \alpha \sin \beta + f_{31} \cos \beta \tag{A84}$$

$$d_{32} = f_{12} \cos \alpha \sin \beta + f_{22} \sin \alpha \sin \beta + f_{32} \cos \beta \tag{A85}$$

$$d_{33} = f_{13} \cos \alpha \sin \beta + f_{23} \sin \alpha \sin \beta + f_{33} \cos \beta \tag{A86}$$

where $f_{ij}$ coefficients are elements of the matrix $BB'^{T}$. The matrix elements of B and B' are known functions of time, and hence the $f_{ij}$ elements are uniquely specified. These elements are computed from the following equations:

$$f_{11} = b_{11}b_{11}' + b_{12}b_{12}' + b_{13}b_{13}' \tag{A87}$$

$$f_{12} = b_{11}b_{21}' + b_{12}b_{22}' + b_{13}b_{23}' \tag{A88}$$

$$f_{13} = b_{11}b_{31}' + b_{12}b_{32}' + b_{13}b_{33}' \tag{A89}$$

$$f_{21} = b_{21}b_{11}' + b_{22}b_{12}' + b_{23}b_{13}' \tag{A90}$$

$$f_{22} = b_{21}b_{21}' + b_{22}b_{22}' + b_{23}b_{23}' \tag{A91}$$

$$f_{23} = b_{21}b_{31}' + b_{22}b_{32}' + b_{23}b_{33}' \tag{A92}$$

$$f_{31} = b_{31}b_{11}' + b_{32}b_{12}' + b_{33}b_{13}' \tag{A93}$$

$$f_{32} = b_{31}b_{21}' + b_{32}b_{22}' + b_{33}b_{23}' \tag{A94}$$

$$f_{33} = b_{31}b_{31}' + b_{32}b_{32}' + b_{33}b_{33}' \tag{A95}$$

Cockpit Instrument and Auxiliary Equations

Target azimuth and elevation with respect to the local vertical axis system is given by

$$\lambda = \tan^{-1} \frac{-y}{-x} \tag{A96}$$

$$\delta = \tan^{-1} \frac{z}{R_{xy}} \tag{A97}$$

where

$$R_{xy} = -(x \cos \lambda + y \sin \lambda) \tag{A98}$$

Range rate is computed for display purposes and is given by

$$\dot{R} = \frac{x\dot{x} + y\dot{y} + z\dot{z}}{\left|\bar{R}_{los}\right|} \tag{A99}$$

where $\left|\bar{R}_{los}\right|$ is defined by equation (A76). The components of $\Delta v$ are computed from the following definitions:

$$\Delta V_X = \frac{1}{m} \int_0^t T_{X,b} \, d\tau \tag{A100}$$

$$\Delta V_Y = \frac{1}{m} \int_0^t T_{Y,b} \, d\tau \tag{A101}$$

$$\Delta V_Z = \frac{1}{m} \int_0^t T_{Z,b} \, d\tau \tag{A102}$$

In these equations, the total mass $m$ is assumed to be constant. The mass changes due to translational and attitude control jets, respectively, are given by

$$\Delta m_{trans} = +\frac{1}{g_e I_{sp}} \int_0^t \left( \left|T_{X+}\right| + \left|T_{X-}\right| + \left|T_{Y+}\right| + \left|T_{Y-}\right| + \left|T_{Z+}\right| + \left|T_{Z-}\right| \right) d\tau \tag{A103}$$

$$\Delta m_{att} = +\frac{1}{g_e I_{sp}} \int_0^t \left( \left|T_{\psi+}\right| + \left|T_{\psi-}\right| + \left|T_{\theta+}\right| + \left|T_{\theta-}\right| + \left|T_{\phi+}\right| + \left|T_{\phi-}\right| \right) d\tau \tag{A104}$$

Thus, the percent fuel used by the translational and attitude control systems are computed as follows:

$$F_{trans} = \frac{\Delta m_{trans}}{F_o} 100 \tag{A105}$$

$$F_{att} = \frac{\Delta m_{att}}{F_o} 100 \tag{A106}$$

where $F_o$ is total fuel initially in kilograms.

## APPENDIX B

## DERIVATION OF GREEN'S FUNCTION TECHNIQUE

This appendix is intended to give a comprehensive derivation of the Green's function technique used in this paper. The motivation for this derivation is that the equation

$$\left(\frac{d^2}{d\tau^2} + 2\zeta_g\omega_g \frac{d}{d\tau} + \omega_g{}^2\right)p_g = \omega_g{}^2 p(\tau) \tag{B1}$$

for the values of $\zeta_g$ and $\omega_g$ for this problem and related problems is difficult to solve by using standard numerical techniques. The difficulty in solving this equation is not the forcing function $p(\tau)$, but is found to be the differential operator on the left-hand side of equation (B1). The approach used in this paper was to find a different linear operator, generically different from the differential operator, with the hope that a more adequate numerical approximation exists for this new operator. Such an operator was found which cast equation (B1) as an integral equation involving Green's function.

The Green's function of equation (B1) satisfies the equation (ref. 19)

$$\left(\frac{d^2}{dt^2} + 2\zeta_g\omega_g \frac{d}{dt} + \omega_g{}^2\right)G(t - \tau) = \omega_g{}^2\delta(t - \tau) \tag{B2}$$

The Green's function also satisfies boundary conditions. These values at the boundaries must be chosen so that a solution to equation (B2) exists and the integral representation of equation (B1) has a simple form.

Multiplying equation (B1) by $G(t - \tau)$ and equation (B2) by $p_g(\tau)$ and subtracting the two results gives

$$G(t - \tau)\left(\frac{d^2}{d\tau^2} + 2\zeta_g\omega_g \frac{d}{d\tau} + \omega_g{}^2\right)p_g(\tau) - p_g(\tau)\left(\frac{d^2}{dt^2} + 2\zeta_g\omega_g{}^2 \frac{d}{dt} + \omega_g{}^2\right)G(t - \tau)$$

$$= \omega_g{}^2\left[G(t - \tau)\, p(\tau) - p_g(\tau)\, \delta(t - \tau)\right] \tag{B3}$$

Integrating equation (B3) on the interval $[0, t + \epsilon]$ results in

$$\omega_g{}^2 \int_0^{t+\epsilon} \left[G(t - \tau)\, p(\tau) - p_g(\tau)\, \delta(t - \tau)\right] d\tau$$

$$= \int_0^{t+\epsilon} \left[G(t - \tau)\left(\frac{d^2}{d\tau^2} + 2\zeta_g\omega_g + \omega_g{}^2\right)p_g(\tau) - p_g(\tau)\left(\frac{d^2}{dt^2} + 2\zeta_g\omega_g \frac{d}{dt} + \omega_g{}^2\right)G(t - \tau)\right] d\tau \tag{B4}$$

## APPENDIX B

Performing the integration of equation (B4) with the delta function yields

$$p_g(t) = \int_0^{t+\epsilon} G(t - \tau)\, p(\tau)\, d\tau + \frac{1}{\omega_g{}^2} \int_0^{t+\epsilon} \left\{ p_g(\tau)\left[\frac{d^2}{dt^2} G(t - \tau)\right] - G(t - \tau)\left[\frac{d^2}{d\tau^2} p_g(\tau)\right]\right\} d\tau$$

$$+ \frac{2\zeta_g}{\omega_g} \int_0^{t+\epsilon} \left\{ p_g(\tau)\left[\frac{d}{dt} G(t - \tau)\right] - G(t - \tau)\left[\frac{d}{d\tau} p_g(\tau)\right]\right\} d\tau \qquad \text{(B5)}$$

Consider the last two integrals of equation (B5). Note that

$$\frac{d}{dt} G(t - \tau) = -\frac{d}{d\tau} G(t - \tau) \qquad \text{(B6)}$$

Then

$$\int_0^{t+\epsilon} \left\{ p_g(\tau)\left[\frac{d}{dt} G(t - \tau)\right] - G(t - \tau)\left[\frac{d}{d\tau} p_g(\tau)\right]\right\} d\tau$$

$$= -\int_0^{t+\epsilon} \left\{ p_g(\tau)\left[\frac{d}{d\tau} G(t - \tau)\right] + G(t - \tau)\left[\frac{d}{d\tau} p_g(\tau)\right]\right\} d\tau$$

$$= -\int_0^{t+\epsilon} \frac{d}{d\tau}\left[p_g(\tau)\, G(t - \tau)\right] d\tau$$

$$= -p_g(\tau)\, G(t - \tau)\Big|_0^{t+\epsilon} \qquad \text{(B7)}$$

The second integral of equation (B5) is evaluated by integrating by parts. Consider

$$\int_0^{t+\epsilon} G(t - \tau)\left[\frac{d^2}{d\tau^2} p_g(\tau)\right] d\tau = G(t - \tau)\left[\frac{d}{d\tau} p(\tau)\right]\Big|_0^{t+\epsilon} - \int_0^{t+\epsilon} \frac{d}{d\tau} p_g(\tau)\, \frac{d}{d\tau} G(t - \tau)\, d\tau \qquad \text{(B8)}$$

Integrating again by parts yields

$$\int_0^{t+\epsilon} G(t - \tau)\left[\frac{d^2}{d\tau^2} p_g(\tau)\right] d\tau = G(t - \tau)\left[\frac{d}{d\tau} p_g(\tau)\right]\Big|_0^{t+\epsilon} - \left[\frac{d}{d\tau} G(t - \tau)\right] p_g(\tau)\Big|_0^{t+\epsilon}$$

$$+ \int_0^{t+\epsilon} p_g(\tau)\left[\frac{d^2}{d\tau^2} G(t - \tau)\right] d\tau \qquad \text{(B9)}$$

By substitution of equation (B6) and the identity

## APPENDIX B

$$\frac{d^2}{dt^2} G(t - \tau) = \frac{d^2}{d\tau^2} G(t - \tau) \tag{B10}$$

equation (B9) becomes

$$\int_0^{t+\epsilon} G(t - \tau)\left[\frac{d^2}{d\tau^2} p_g(\tau)\right] d\tau = G(t - \tau)\left[\frac{d}{d\tau} p_g(\tau)\right]\Bigg|_0^{t+\epsilon} + \left[\frac{d}{dt} G(t - \tau)\right] p_g(\tau)\Bigg|_0^{t+\epsilon}$$

$$+ \int_0^{t+\epsilon} p_g(\tau)\left[\frac{d^2}{dt^2} G(t - \tau)\right] d\tau \tag{B11}$$

Substituting these results (eqs. (B7) and (B11)) into equation (B5) yields

$$p_g(t) = \int_0^{t+\epsilon} G(t - \tau)\, p(\tau)\, d\tau - \frac{1}{\omega_g{}^2}\left\langle G(t - \tau)\frac{d}{d\tau} p_g(\tau) + \left[\frac{d}{dt} G(t - \tau)\right] p_g(\tau)\right\rangle\Bigg|_0^{t+\epsilon}$$

$$- \frac{2\zeta_g}{\omega_g} p_g(\tau)\, G(t - \tau)\Bigg|_0^{t+\epsilon} \tag{B12}$$

Evaluating the algebraic expressions at their limits and grouping yields

$$p_g(t) = \int_0^{t+\epsilon} G(t - \tau)\, p(\tau)\, d\tau$$

$$- \frac{1}{\omega_g}\left\langle \frac{1}{\omega_g}\left[G(-\epsilon)\, \dot{p}_g(t + \epsilon) + \dot{G}(-\epsilon)\, p_g(t + \epsilon)\right] + 2\zeta_g G(-\epsilon)\, p_g(t + \epsilon)\right\rangle$$

$$+ \frac{1}{\omega_g}\left\langle \frac{1}{\omega_g}\left[G(t)\, \dot{p}_g(0) + \dot{G}(t)\, p_g(0)\right] + 2\zeta_g G(t)\, p_g(0)\right\rangle \tag{B13}$$

with the convention that $\dot{f}(x) = \lim_{y \to x} \frac{df(y)}{dy}$. Therefore a solution to equation (B2) is needed which satisfies the following conditions:

$$\left.\begin{aligned} &G(t) = 0 \qquad (t \leqq 0) \\ &\lim_{t \to 0} \dot{G}(-t) = 0 \\ &\dot{G}(0) = \omega_g{}^2 \\ &\lim_{t \to \infty} G(t) = \lim_{t \to \infty} \dot{G}(t) = 0 \end{aligned}\right\} \tag{B14}$$

## APPENDIX B

Taking the limit of equation (B13) as $\epsilon$ goes to zero yields

$$p_g(t) = \int_0^t G(t - \tau)\, p(\tau)\, d\tau + \left[\frac{1}{\omega_g{}^2}\dot{G}(t) + \frac{2\zeta_g}{\omega_g}G(t)\right] p_g(0) + \frac{1}{\omega_g{}^2}G(t)\, \dot{p}_g(0) \qquad \text{(B15)}$$

Adding the further restriction on the Green's function yields

$$\ddot{G}(0) + 2\zeta_g\omega_g\dot{G}(0) = 0 \qquad \text{(B16)}$$

The boundary conditions given by equations (B14) and (B16) are needed for the solution to have a simple form (eq. (B15)) which satisfies the initial conditions of $p_g(t)$. A solution to equation (B2) must be found which satisfies these boundary conditions, that is, if such a solution even exists.

The existence of the Green's function is shown by finding a solution to equation (B2) which satisifes equation (B14) and equation (B16). Consider the equation

$$\left(\frac{d^2}{dt^2} + 2\zeta_g\omega_g\frac{d}{dt} + \omega_g{}^2\right) G(t) = \omega_g{}^2\, \delta(t) \qquad \text{(B17)}$$

Taking the Laplace transform $s$ of equation (B17) (ref. 19) yields

$$\left(s^2 + 2\zeta_g\omega_g s + \omega_g{}^2\right) G^*(s) = \omega_g{}^2 \qquad \text{(B18)}$$

from which $G^*(s)$ is found, as expected, to be the transfer function of equation (B1)

$$G^*(s) = \frac{\omega_g{}^2}{s^2 + 2\zeta_g\omega_g s + \omega_g{}^2} \qquad \text{(B19)}$$

The inverse Laplace of $G^*(s)$ can be found in standard tables to be

$$G(t) = \frac{\omega_g{}^2}{\Gamma}e^{-\xi t}\sin \Gamma t \qquad (t \geqq 0) \qquad \text{(B20)}$$

where $\xi = \zeta_g\omega_g$ and $\Gamma = \omega_g\left(1 - \zeta_g{}^2\right)^{1/2}$. The first two derivatives of equation (B20) are

$$\dot{G}(t) = -\xi G(t) + \omega_g{}^2 e^{-\xi t}\cos \Gamma t \qquad \text{(B21)}$$

$$\ddot{G}(t) = -\xi\dot{G}(t) - \xi\omega_g{}^2 e^{-\xi t}\cos \Gamma t - \Gamma^2 G(t) \qquad \text{(B22)}$$

for $t \geq 0$ and by equations (B14)

$$\dot{G}(t) = \ddot{G}(t) = 0 \qquad (t < 0)$$

Hence, the following boundary conditions hold:

$$G(0) = 0$$

$$\lim_{t \to 0} \dot{G}(-t) = 0$$

$$\dot{G}(0) = \omega_g{}^2$$

$$\lim_{t \to \infty} G(t) = \lim_{t \to \infty} \dot{G}(t) = 0$$

From equation (B22)

$$\ddot{G}(0) = -\xi \dot{G}(0) - \xi \omega_g{}^2 = -2\zeta_g \omega_g \dot{G}(0)$$

Thus, the Green's function of equation (B20) meets all the requirements of equations (B14) and (B16).

In determining equation (B15), no assumptions were made of the form of $p(\tau)$. Equation (B15) is a valid solution even when $p(\tau)$ is a nonlinear function of $p_g$.

The remainder of this appendix is centered on the evaluation of the integral. Normally, initial conditions are zero which is consistent with the usage in the text. Initial conditions can be incorporated in the resulting integration scheme; this procedure is shown later in the appendix. Equation (B15) with zero initial conditions is

$$p_g(t) = \int_0^t G(t - \tau)\, p(\tau)\, d\tau \qquad (B23)$$

which is not in a useful form. The solution would require storage of the forcing function from the beginning of the problem and the evaluation of a rather complex integral over increasingly large ranges as the problem progressed. For an efficient integration of equation (B23), a form needed to be found so that only local information of the forcing function and values of the integral are needed to propagate the solution. To find such a form, consider $p_g(t)$ to be known at time $t$ and $p(\tau)$ specified on the interval $(t, t + h)$ and look at equation (B23) at time $t + h$; then,

$$p_g(t + h) = \int_0^{t+h} G(t + h - \tau)\, p(\tau)\, d\tau \qquad (B24)$$

## APPENDIX B

Note that

$$G(t + h - \tau) = \frac{\Gamma}{\omega_g^2}\left[G^\dagger(h)\, G(t - \tau) + G(h)\, G^\dagger(t - \tau)\right] \tag{B25}$$

where

$$G^\dagger(t) = \frac{\omega_g^2}{\Gamma} e^{-\xi t} \cos \Gamma t$$

Equation (B24) is then

$$p_g(t + h) = \frac{\Gamma}{\omega_g^2} G^\dagger(h) \int_0^{t+h} G(t - \tau)\, p(\tau)\, d\tau + \frac{\Gamma}{\omega_g^2} G(h) \int_0^{t+h} G^\dagger(t - \tau)\, p(\tau)\, d\tau$$

$$= \frac{\Gamma}{\omega_g^2} G^\dagger(h)\left[\int_0^t G(t - \tau)\, p(\tau)\, d\tau + \int_t^{t+h} G(t - \tau)\, p(\tau)\, d\tau\right]$$

$$+ \frac{\Gamma}{\omega_g^2} G(h)\left[\int_0^t G^\dagger(t - \tau)\, p(\tau)\, d\tau + \int_t^{t+h} G^\dagger(t - \tau)\, p(\tau)\, d\tau\right] \tag{B26}$$

where equation (B26) has the form of an integration over the last interval with the addition of previously computed information provided the auxiliary computation

$$\Lambda(t) = \int_0^t G^\dagger(t - \tau)\, p(\tau)\, d\tau \tag{B27}$$

is made.

The computation of equation (B27) can be placed in a similar form by using the same process. Consider

$$\Lambda(t + h) = \int_0^{t+h} G^\dagger(t + h - \tau)\, p(\tau)\, d\tau \tag{B28}$$

where

$$G^\dagger(t + h - \tau) = \frac{\Gamma}{\omega_g^2} G^\dagger(h)\, G^\dagger(t - \tau) - \frac{\Gamma}{\omega_g^2} G(h)\, G(t - \tau) \tag{B29}$$

Equation (B28) can then be written

$$\Lambda(t + h) = \frac{\Gamma}{\omega_g^2} G^\dagger(h)\left[\int_0^t G^\dagger(t - \tau)\, p(\tau)\, d\tau + \int_t^{t+h} G^\dagger(t - \tau)\, p(\tau)\, d\tau\right]$$

$$- \frac{\Gamma}{\omega_g^2} G(h)\left[\int_0^t G(t - \tau)\, p(\tau)\, d\tau + \int_t^{t+h} G(t - \tau)\, p(\tau)\, d\tau\right] \tag{B30}$$

Substituting equations (B27) and (B23) into equations (B26) and (B30) and writing the result as a matrix product results in

$$\begin{bmatrix} p_g(t+h) \\ \Lambda(t+h) \end{bmatrix} = \frac{\Gamma}{\omega_g^2} \begin{bmatrix} G^\dagger(h) & G(h) \\ -G(h) & G^\dagger(h) \end{bmatrix} \begin{bmatrix} p_g(t) + \int_t^{t+h} G(t-\tau)\, p(\tau)\, d\tau \\ \Lambda(t) + \int_t^{t+h} G^\dagger(t-\tau)\, p(\tau)\, d\tau \end{bmatrix} \tag{B31}$$

To this point no approximations or assumptions have been made. The solution is valid and almost in a form to be realized on a digital computer. At this point many variations of the evaluation of the integrals leading to various numerical techniques can be made. An example is the approximation for $p(\tau)$ on $I(t, t+h)$ of

$$p(\tau) \approx p(\tau)\ \delta(t-\tau) \tag{B32}$$

which leads to the primitive recursive filter. (See ref. 5.) In this application $p(\tau)$ is known to the accuracy of the integration scheme in the moment equations where $p(\tau)$ is computed. Hence, $p(\tau)$ is known to be some polynomial on $I(t, t+h)$:

$$p(\tau) = a + b\tau + c\tau^2 + \ldots f\tau^n \tag{B33}$$

Within this framework, equations (B31) can be evaluated exactly (at least within computer accuracy). To do this, first change the integration variable by the transformation

$$x = \tau - t \tag{B34}$$

Thus,

$$dx = d\tau \tag{B35}$$

and equations (B31) become

$$\begin{bmatrix} p_g(t+h) \\ \Lambda(t+h) \end{bmatrix} = \frac{\Gamma}{\omega_g^2} \begin{bmatrix} G^\dagger(h) & G(h) \\ -G(h) & G^\dagger(h) \end{bmatrix} \begin{bmatrix} p_g(t) + \int_0^h G(-x)\, p(t+x)\, dx \\ \Lambda(t) + \int_0^h G^\dagger(-x)\, p(t+x)\, dx \end{bmatrix} \tag{B36}$$

and equation (B33) becomes

$$p(t+x) = \sum_{j=0}^{n} a_j x^j \tag{B37}$$

Substituting equation (B37) into equations (B36) yields

$$\begin{bmatrix} p_g(t+h) \\ \Lambda(t+h) \end{bmatrix} = \frac{\Gamma}{\omega_g{}^2} \begin{bmatrix} G^\dagger(h) & G(h) \\ -G(h) & G^\dagger(h) \end{bmatrix} \begin{bmatrix} p_g(t) + \sum_{j=0}^{n} a_j I_j \\ \Lambda(t) + \sum_{j=0}^{n} a_j I_j{}^\dagger \end{bmatrix} \tag{B38}$$

where

$$I_j = \int_0^h G(-x)x^j \, dx$$

$$I_j{}^\dagger = \int_0^h G^\dagger(-x)x^j \, dx$$

for $j = 0, 1, 2 \ldots$. Rewriting equation (B21) in terms of $G(t)$ and $G^\dagger(t)$

$$\dot{G}(t) = -\xi G(t) + \Gamma G^\dagger(t) \tag{B39}$$

so that

$$\dot{G}(t) + 2\zeta_g \omega_g G(t) = \Gamma G^\dagger(t) + \xi G(t) \tag{B40}$$

Neglecting the integral part of equation (B15) results in

$$p_g(t) = \left[\frac{\Gamma}{\omega_g{}^2} G^t(t) + \frac{\xi}{\omega_g{}^2} G(t)\right] p_g(0) + \frac{1}{\omega_g{}^2} G(t) \, \dot{p}_g(0) \tag{B41}$$

Advancing equation (B41) in time results in

$$\begin{aligned} p_g(t+h) &= \frac{\Gamma}{\omega_g{}^2} p_g(0) \, G^t(t+h) + \left[\frac{\xi}{\omega_g{}^2} p_g(0) + \frac{1}{\omega_g{}^2} \dot{p}_g(0)\right] G(t+h) \\ &= \frac{\Gamma}{\omega_g{}^2} p_g(0) \left[G^t(h) \, G^t(t) - G(h) \, G(t)\right] \\ &\quad + \left[\frac{\xi}{\omega_g{}^2} p_g(0) + \frac{1}{\omega_g{}^2} \dot{p}_g(0)\right] \left[G^t(h) \, G(t) + G(h) \, G^t(t)\right] \end{aligned} \tag{B42}$$

## APPENDIX B

Grouping terms in equation (B42) gives

$$p_g(t+h) = \frac{\Gamma}{\omega_g^2} G^t(h)\left\{\left[\frac{\Gamma}{\omega_g^2} G^t(t) + \frac{\xi}{\omega_g^2} G(t)\right] p_g(0) + \frac{1}{\omega_g^2}\dot{p}_g(0)\ G(t)\right\}$$

$$+ \frac{\Gamma}{\omega_g^2} G(h)\left\{\left[\frac{\xi}{\omega_g^2} G^t(t) - \frac{\Gamma}{\omega_g^2} G(t)\right] p_g(0) + \frac{1}{\omega_g^2}\dot{p}_g(0)\ G^t(t)\right\} \qquad \text{(B43)}$$

Comparison of equation (B43) with (B38) yields for $p(t) = 0$

$$\lambda(t) = \left[\frac{\xi}{\omega_g^2} G^t(t) - \frac{\Gamma}{\omega_g^2} G(t)\right] p_g(0) + \frac{1}{\omega_g^2}\dot{p}_g(0)\ G^t(t) \qquad \text{(B44)}$$

The initial conditions to start the integration scheme (eqs. (B38)) are then

$$p_g(0) = p_g(0)$$

$$\lambda(0) = \frac{\xi}{\Gamma} p_g(0) + \frac{1}{\Gamma}\dot{p}_g(0)$$

## REFERENCES


1. Connelly, Mark E.: Real-Time Analog-Digital Computation. Simulation, vol. 1, no. 1, Fall 1963, pp. R29-R39.

2. Krasny, Louis M.: The Functional Design of a Special-Purpose Digital Computer for Real-Time Flight Simulation. MRL-TDR-62-39, U.S. Air Force, Apr. 1962.

3. Havranek, W. A.: Digital Computers in Flight Simulation. World Aerosp. Syst., vol. 1, no. 5, May 1965, pp. 248-252.

4. Boxer, Rubin; and Thaler, Samuel: Extensions of Numerical Transform Theory. RADC-TR-56-115, DDC No. AD 97793, U.S. Air Force, Nov. 1956.

5. Baxter, D. C.: Digital Simulation Using Approximate Methods. N.R.C. No. 8630 (MK-15), Nat. Res. Counc. Can. (Ottawa), July 1965.

6. Trauboth, Heinz H.: Digital Simulation of General Control Systems. Simulation, vol. 8, no. 6, June 1967, pp. 319-329.

7. Fowler, Maury E.: A New Numerical Method for Simulation. Simulation, vol. 4, no. 5, May 1965, pp. 324-330.

8. Kozak, W. S.; Burns, A.; Fischthal, M.; Greene, J.; Hunter, J.; Kane, P.; Kelly, M.; and McIntyre, A.: Full Mission Engineering Simulator (FMES), Computer Capacity Report. Part II – Programming Analysis and Computer Sizing. Rep. No. LED-570-7, Grumman Aircraft Eng. Corp., Jan. 31, 1964.

9. Korn, Granino A.; and Korn, Theresa M.: Electronic Analog and Hybrid Computers. McGraw-Hill Book Co., c.1964.

10. Mechtly, E. A.: The International System of Units – Physical Constants and Conversion Factors. NASA SP-7012, 1964.

11. Adams, James J.; and Moen, Gene C.: Station Keeping Studies. AIAA Paper No. 67-617, Aug. 1967.

12. Williams, James R.; and Adams, James J.: Investigation of Tethered Station Keeping. NASA TN D-4258, 1967.

13. Fogel, L. J.; and Moore, Roger A.: Modeling the Human Operator With Finite-State Machines. NASA CR-1112, 1968.

14. Jury, E. I.: Theory and Application of the z-Transform Method. John Wiley & Sons, Inc., c.1964.

15. Henrici, Peter: Discrete Variable Methods in Ordinary Differential Equations. John Wiley & Sons, Inc., c.1962.

16. Henrici, Peter: Elements of Numerical Analysis. John Wiley & Sons, Inc., c.1964.

17. Henrici, Peter: Error Propagation for Difference Methods. John Wiley & Sons, Inc., c.1963.

18. Stanton, Ralph G.: Numerical Methods for Science and Engineering. Prentice-Hall, Inc., c.1961.

19. Mathews, Jon; and Walker, R. L.: Mathematical Methods of Physics. W. A. Benjamin, Inc., 1964.

20. Pipes, Louis A.: Operational Methods in Nonlinear Mechanics. Dover Publ., Inc., c.1965.

21. Giese, Clarence: State Variable Difference Methods for Digital Simulation. Simulation, vol. 8, no. 5, May 1967, pp. 263-271.

TABLE I.- ROOT LOCATIONS FOR EULER PARAMETERS AND DIRECTION COSINES

| Parameter | Laplace | | Adams-Bashforth | | Euler | |
|---|---|---|---|---|---|---|
| | Time constant | Frequency | Time constant | Frequency | Time constant | Frequency |
| Euler parameters | $\infty$ | $\omega/2$ | From equation (69) | | From equation (64) | |
| | | | $\frac{1}{4}\frac{256}{h^3\omega^4}$ | $\frac{\omega}{2}+\frac{5}{96}h^2\omega^3$ | $\frac{8}{h\omega^2}$ | $\frac{\omega}{2}-\frac{h^2\omega^3}{24}$ |
| Direction cosines | $\infty$ | $\omega$ | From equation (59) | | From equation (41) | |
| | | | $\frac{1}{4}\frac{16}{h^3\omega^4}$ | $\omega+\frac{5}{12}h^2\omega^3$ | $\frac{2}{h\omega^2}$ | $\omega-\frac{h^2\omega^3}{3}$ |

TABLE II.- ROUNDOFF AND TRUNCATION ERRORS

IN TRANSLATIONAL VARIABLES

| Source | $\rho$ | $\theta$, radians | x, meters | z, meters |
|---|---|---|---|---|
| Time, 1008 sec | | | | |
| Double precision Runge-Kutta (4th order) | -0.00299817 | 1.1991391 | -1179.7356 | -1381.6586 |
| Partial double precision Adams-Bashforth (2d order) | -.00299817 | 1.1991391 | -1179.7333 | -1381.6559 |
| Single precision Adams-Bashforth (2d order) | -.00299756 | 1.1990303 | -1179.5947 | -1381.3930 |
| Time, 2004 sec | | | | |
| Double precision Runge-Kutta (4th order) | -0.01266422 | 2.3510946 | 1990.8761 | -1055.6684 |
| Partial double precision Adams-Bashforth (2d order) | -.01266422 | 2.3510947 | 1990.8720 | -1055.6661 |
| Single precision Adams-Bashforth (2d order) | -.01266017 | 2.3506772 | 1990.1228 | -1055.2903 |
| Time, 3000 sec | | | | |
| Double precision Runge-Kutta (4th order) | -0.01626021 | 3.4786051 | -2717.4585 | 486.8879 |
| Partial double precision Adams-Bashforth (2d order) | .01626021 | 3.4786052 | -2717.4524 | 486.8873 |
| Single precision Adams-Bashforth (2d order) | .01625222 | 3.4777238 | -2715.9020 | 486.6915 |
| Time, 4008 sec | | | | |
| Double precision Runge-Kutta (4th order) | 0.00346380 | 4.6313472 | -148.1033 | 1474.5843 |
| Partial double precision Adams-Bashforth (2d order) | .00346380 | 4.6313472 | -148.1018 | 1474.5815 |
| Single precision Adams-Bashforth (2d order) | .00346282 | 4.6297367 | -147.7157 | 1473.6415 |
| Time, 5004 sec | | | | |
| Double precision Runge-Kutta (4th order) | -0.01052772 | 5.8052815 | -2703.0378 | 681.0652 |
| Partial double precision Adams-Bashforth (2d order) | -.01052772 | 5.8052815 | -2703.0333 | 681.0635 |
| Single precision Adams-Bashforth (2d order) | -.01051593 | 5.8027082 | -2701.1182 | 680.5329 |

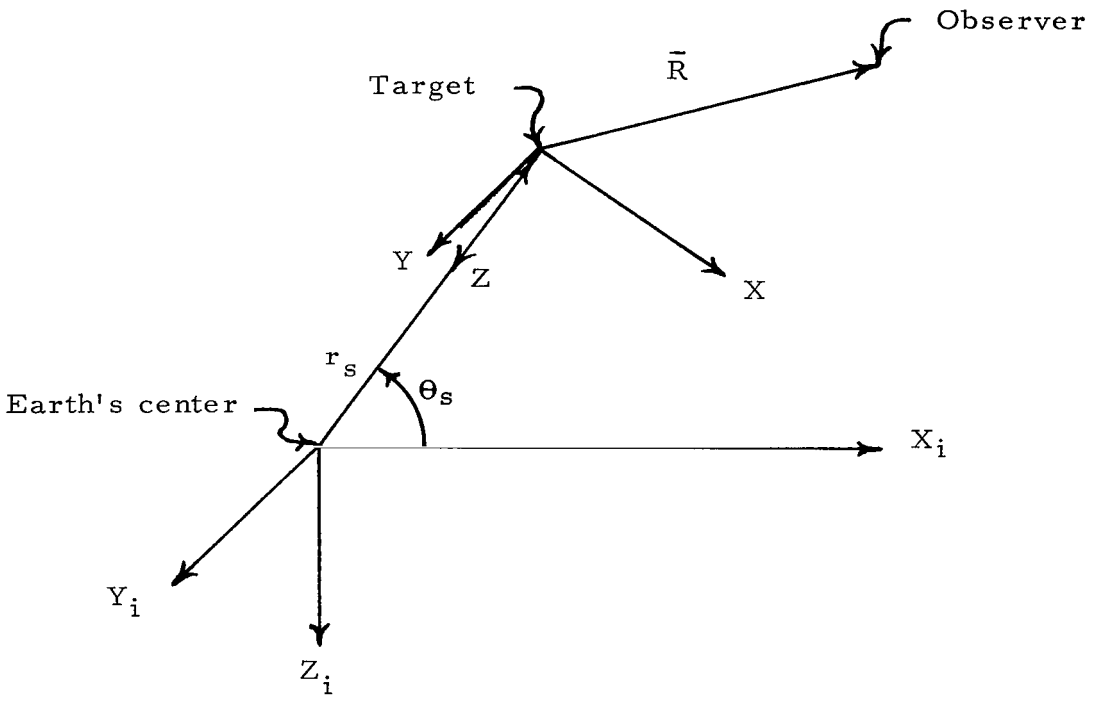


Figure 1.- Basic coordinate systems and relative geometry of target and observer vehicles relative to a geocentric coordinate frame.

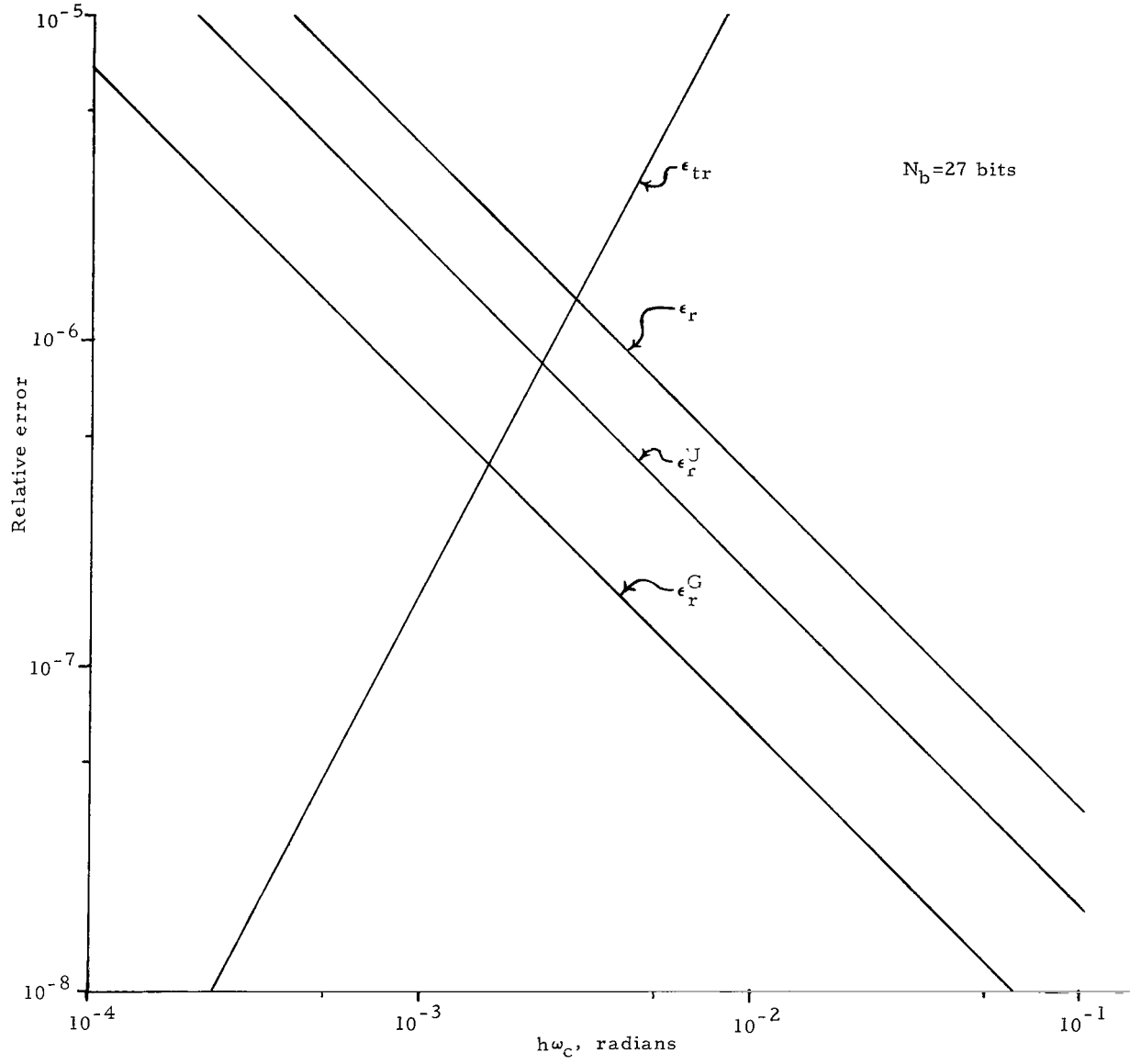


Figure 2.- Local relative roundoff and truncation errors as a function of frequency and interval size for second-order techniques on a 27-bit fractional part machine.

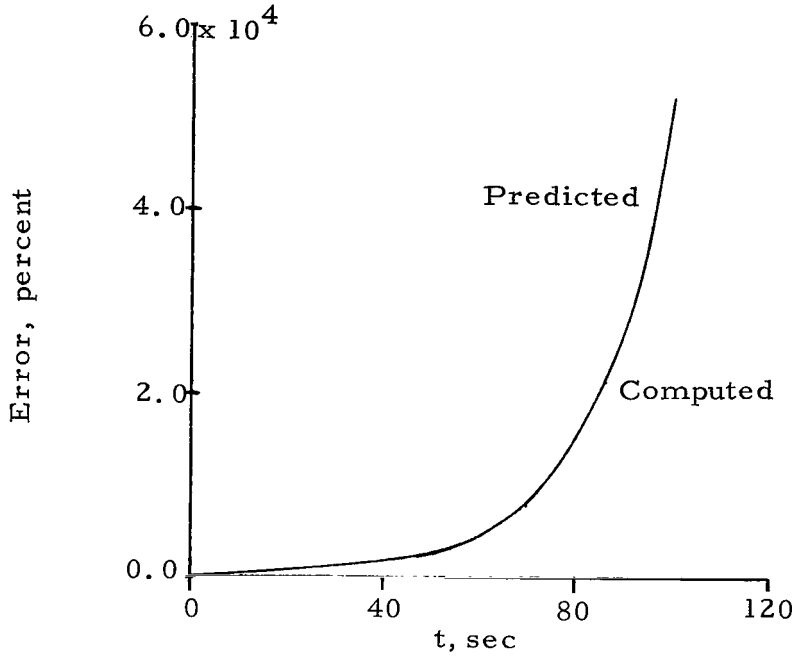


Figure 3.- Predicted and computed errors in the norm of the direction cosines for $p = q = r = \frac{1}{\sqrt{3}}$ radian/second and $h = \frac{1}{16}$ second using Euler integration.

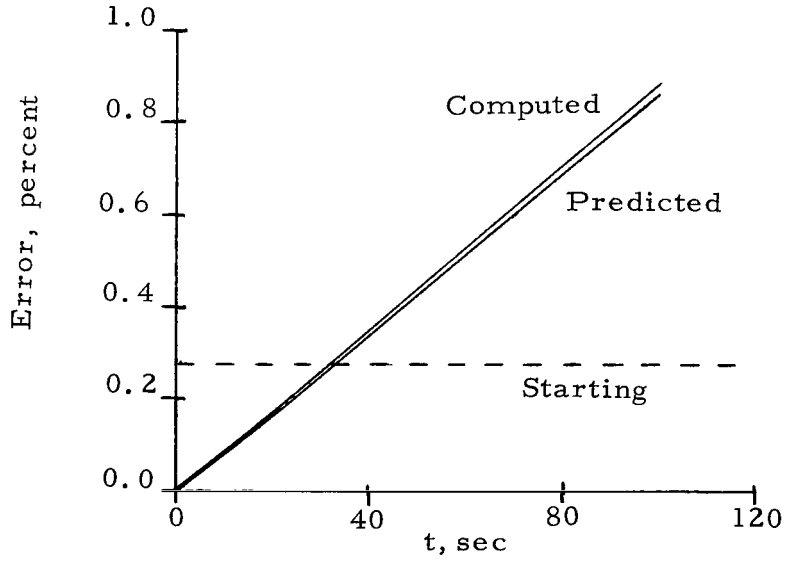


Figure 4.- Predicted, computed, and starting errors in the norm of the direction cosines for $p = q = r = \frac{1}{\sqrt{3}}$ radian/second and $h = \frac{1}{16}$ second using Adams-Bashforth second-order integration with Euler integration as starting formula.

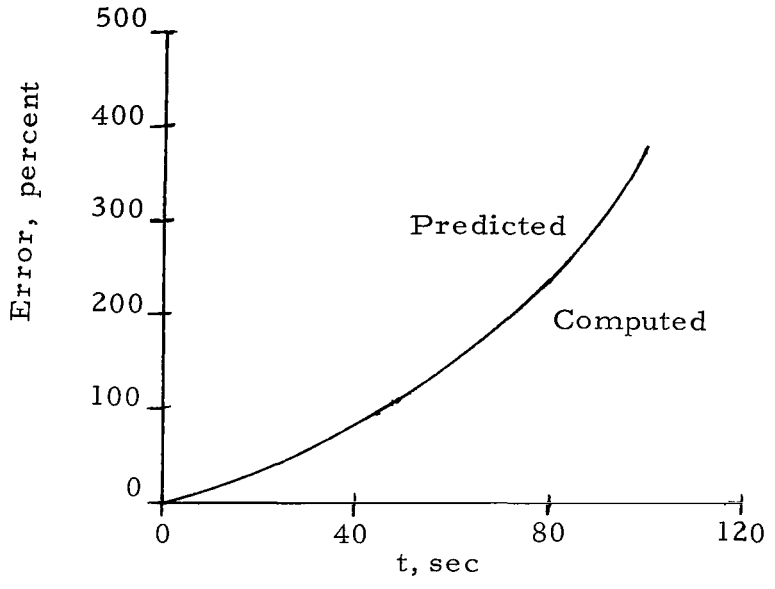


Figure 5.- Predicted and computed errors in norm of the Euler parameters for $p = q = r = \frac{1}{\sqrt{3}}$ radian/second and $h = \frac{1}{16}$ second using Euler integration.

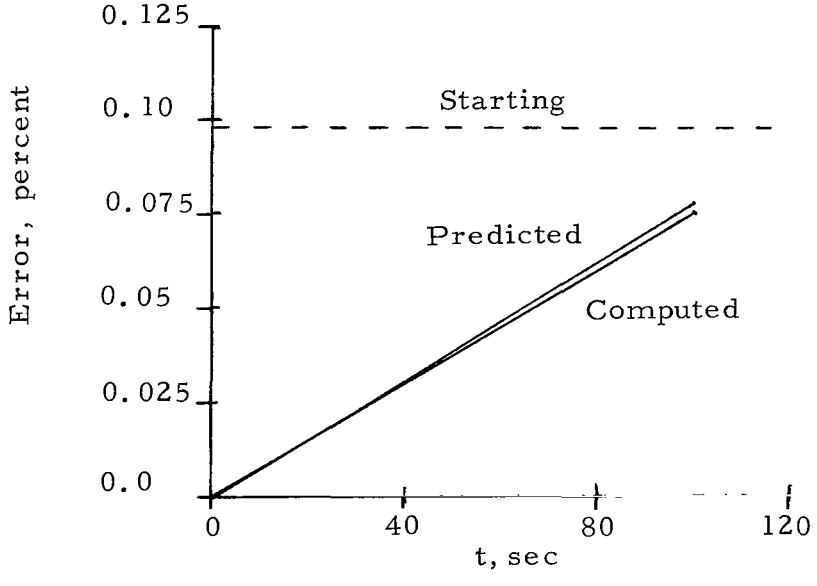


Figure 6.- Predicted, computed, and starting errors in norm of the Euler parameters for $p = q = r = \frac{1}{\sqrt{3}}$ radian/second and $h = \frac{1}{16}$ second using Adams-Bashforth second-order integration with Euler integration as starting formula.

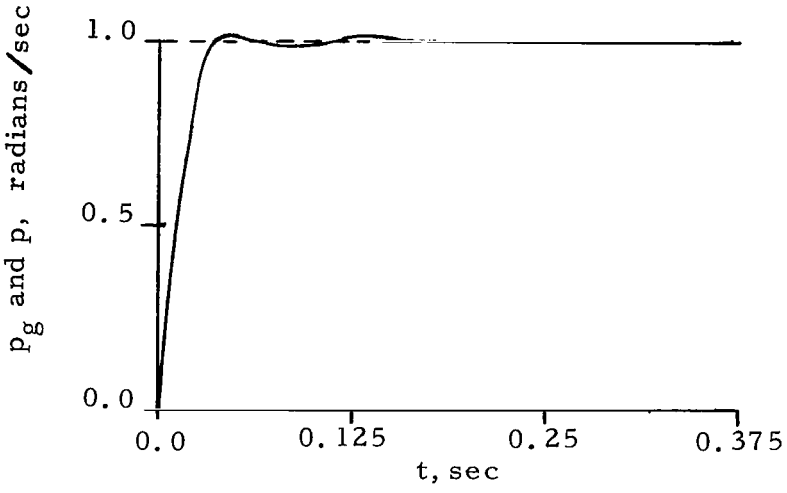


Figure 7.- Gyroscope response (solid) to a step input (dashed) for $\omega_g$ = 125 radians/second and $\zeta_g$ = 0.8 with h = $\frac{1}{64}$ and $\frac{1}{32}$ second using the Green's function technique.

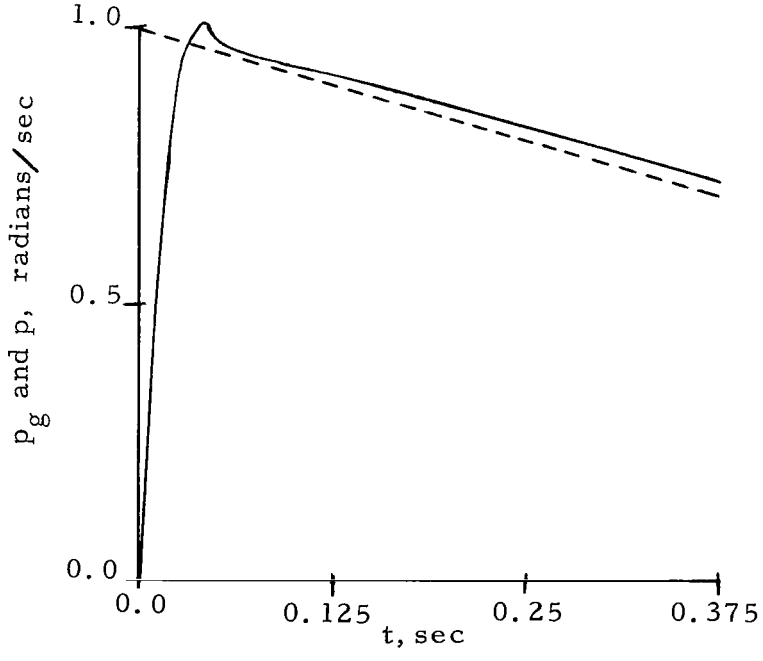


Figure 8.- Gyroscope response (solid) to a ramp input (dashed) for $\omega_g$ = 125 radians/second and $\zeta_g$ = 0.8 with h = $\frac{1}{64}$ and $\frac{1}{32}$ second using the Green's function technique.

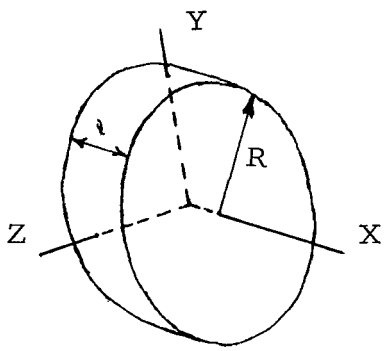


Figure 9.- Cylindrical shape of uniform density showing location of axes.

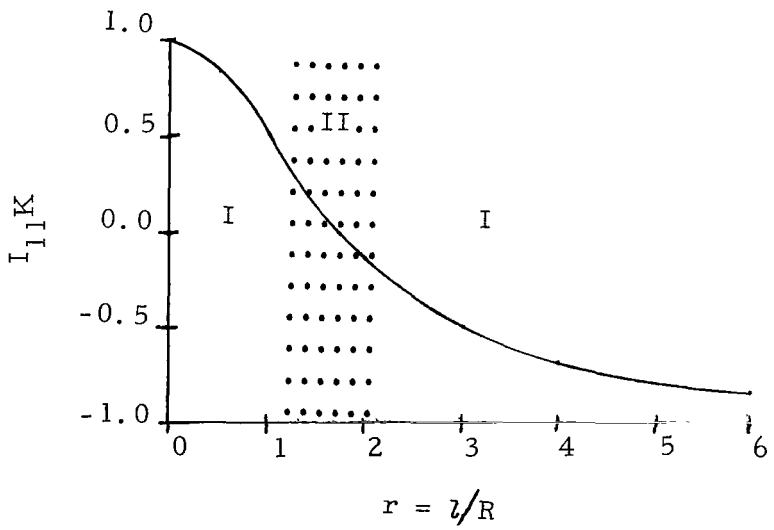


Figure 10.- $I_{11}K$ as function of the ratio $r$ of length $l$ to the radius R. Regions I and II refer to the linear and nonlinear regions, respectively.

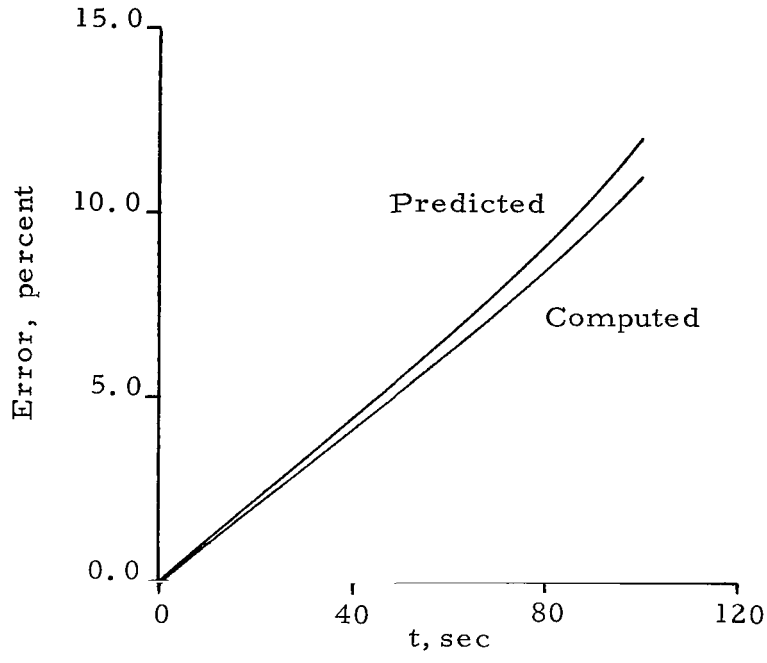


Figure 11.- Predicted and computed errors in total angular momentum for $I_{11}$ = 500.0 kg-m$^2$, $I_{22}$ = 878.9 kg-m$^2$, $I_{33}$ = 881.9 kg-m$^2$, p = q = r = $\frac{1}{\sqrt{3}}$ radian/second and h = $\frac{1}{32}$ second using Euler integration.

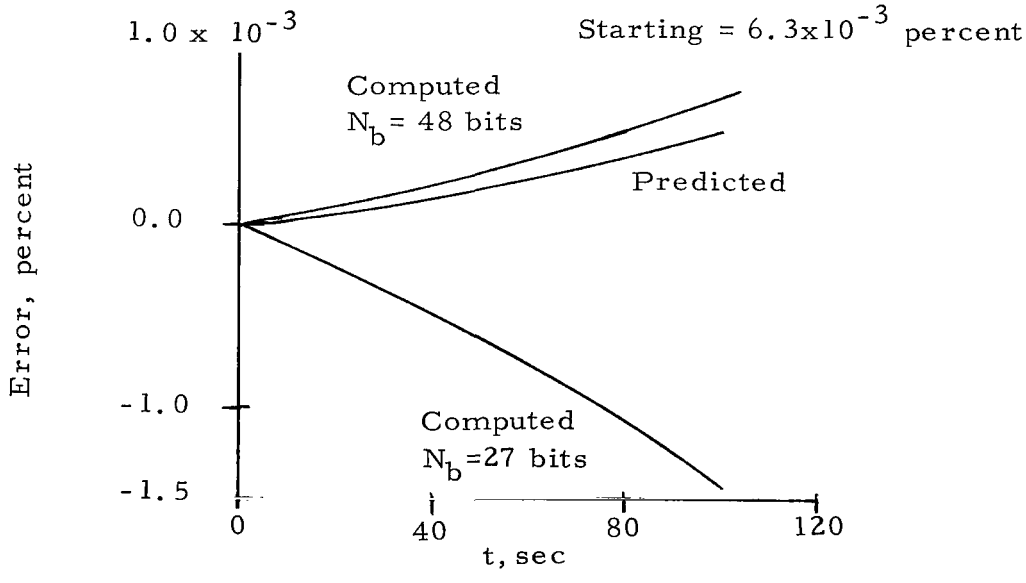


Figure 12.- Predicted, computed, and starting errors in total angular momentum for $I_{11}$ = 500.0 kg-m$^2$, $I_{22}$ = 878.9 kg-m$^2$, $I_{33}$ = 881.9 kg-m$^2$, p = q = r = $\frac{1}{\sqrt{3}}$ radian/second and h = $\frac{1}{32}$ second using Adams-Bashforth second-order integration with Euler integration as starting formula.

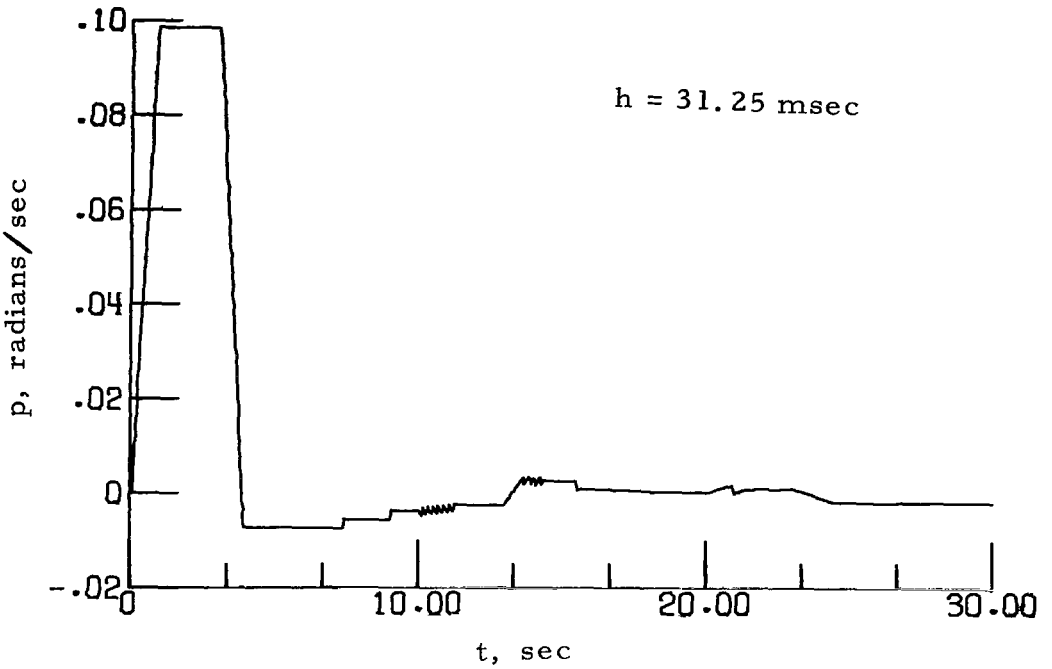


(a) h = 31.25 msec.

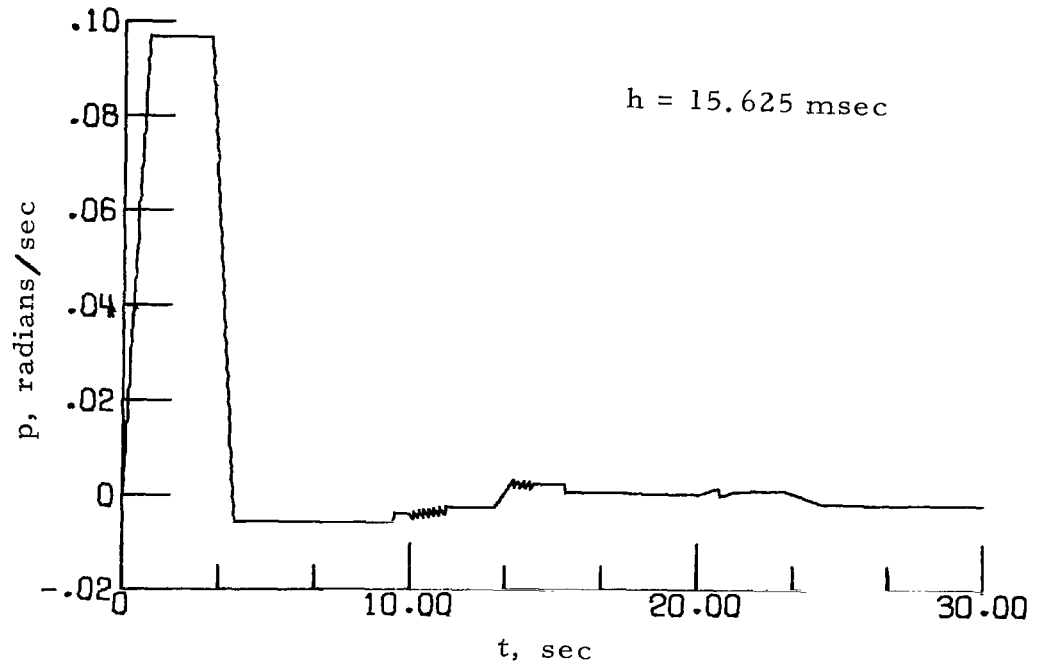


(b) h = 15.625 msec.

Figure 13.- Time-history plot of p for attitude control step input.

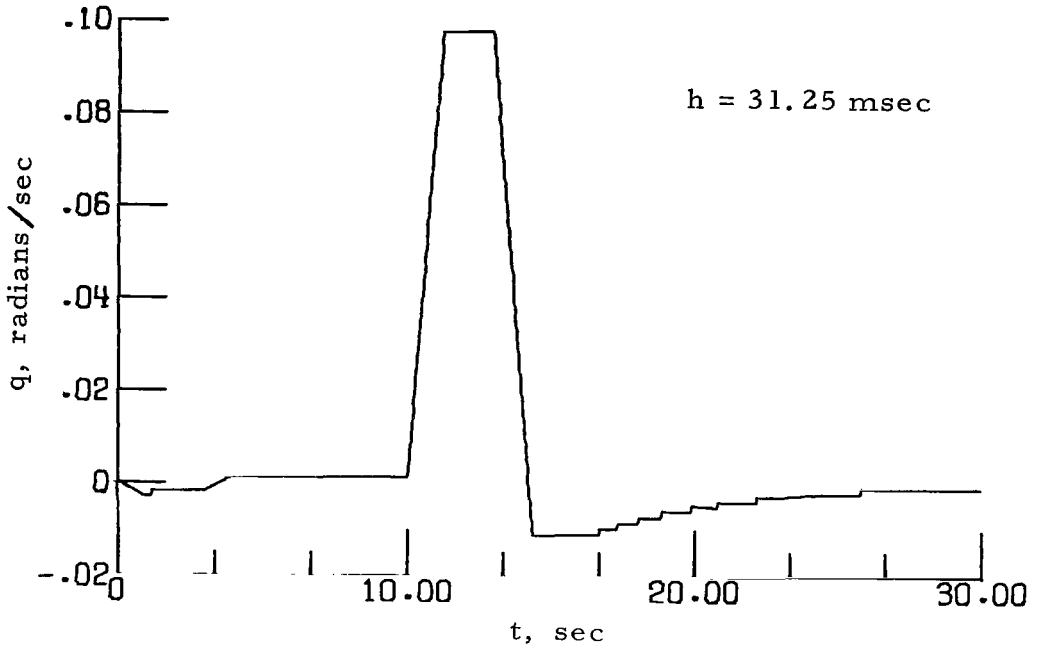


(a) h = 31.25 msec.

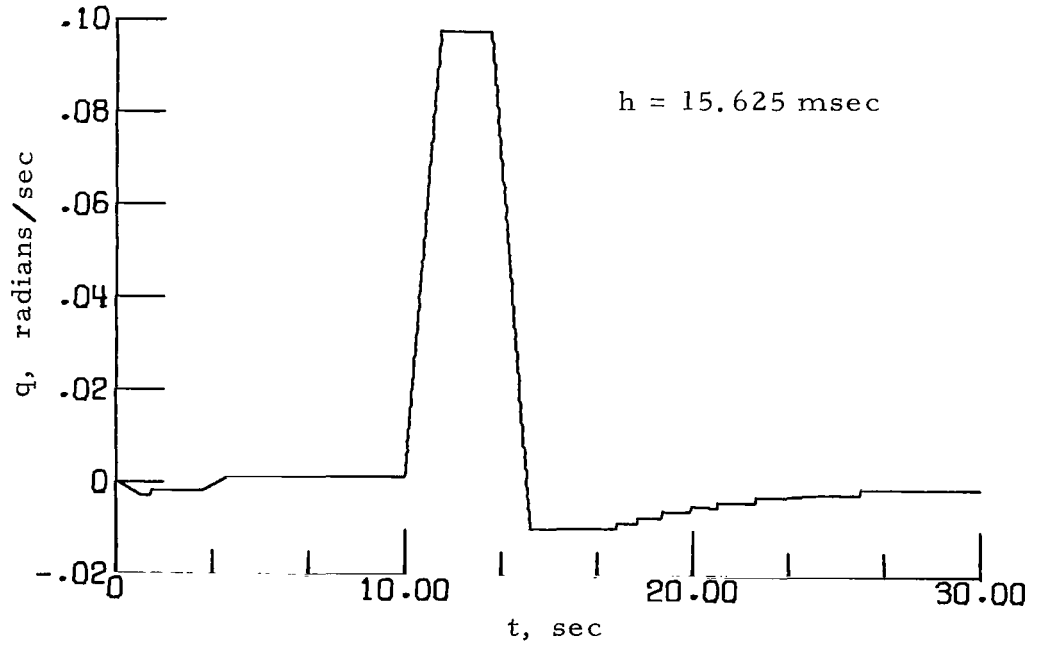


(b) h = 15.625 msec.

Figure 14.- Time-history plot of q for attitude control step input.

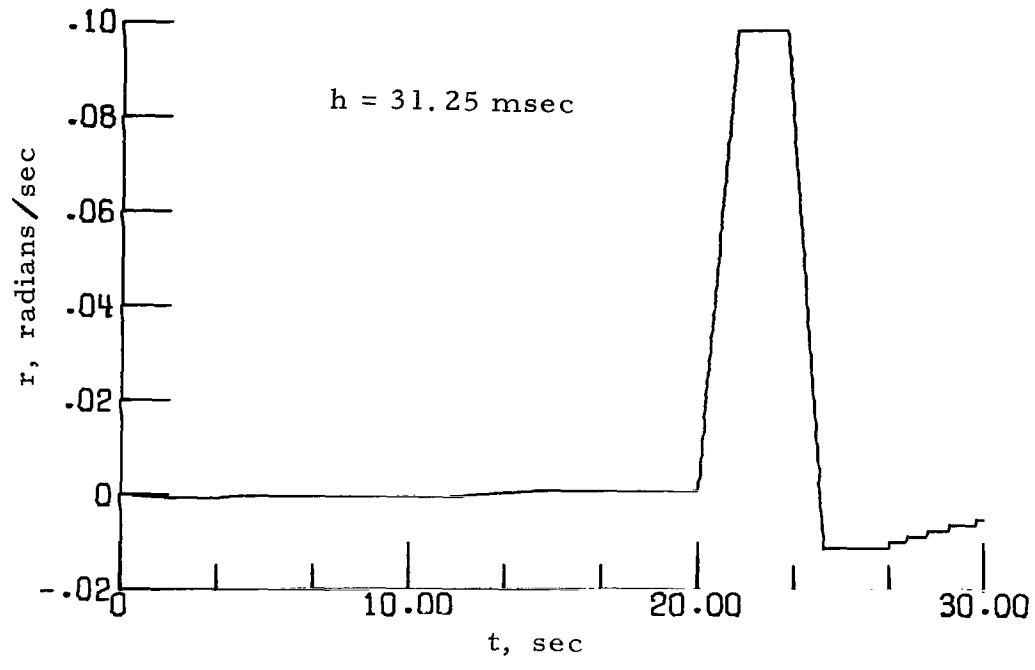


(a) h = 31.25 msec.

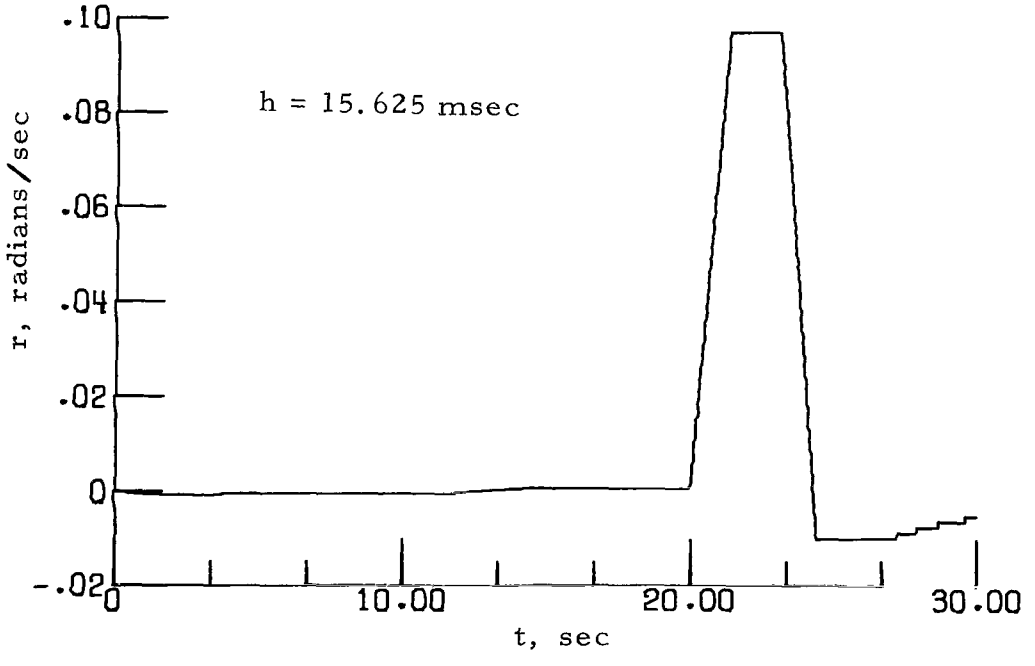


(b) h = 15.625 msec.

Figure 15.- Time-history plot of r for attitude control step input.

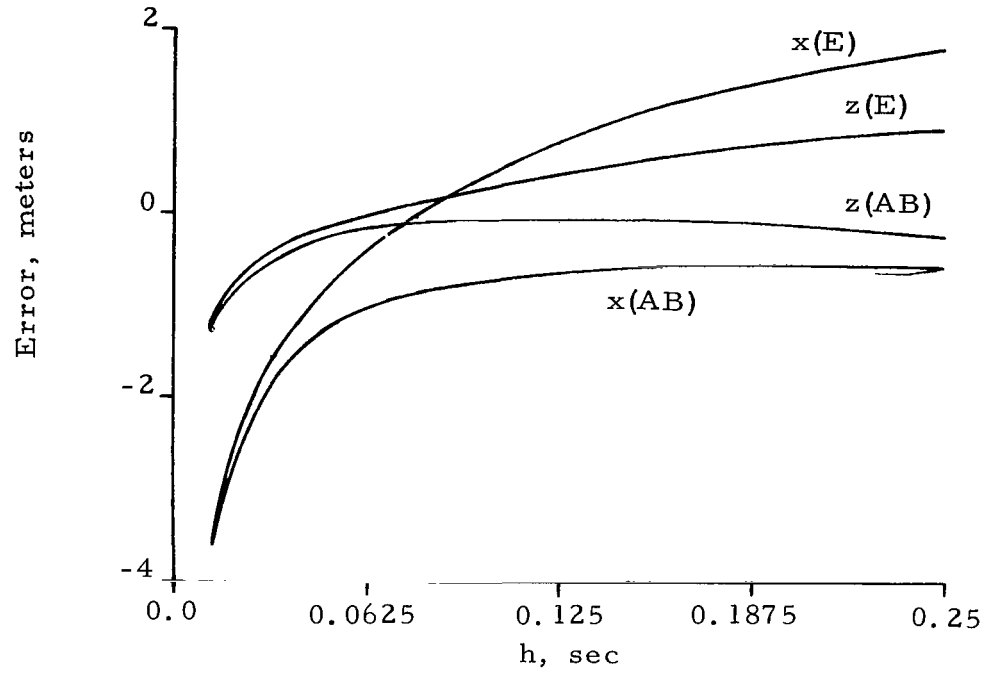


Figure 16.- Global error as function of step size h in trajectory variables at t = 5004 seconds for Euler (E) and Adams-Bashforth (AB) second-order integration over the range $\frac{1}{64}$ second $\leq h \leq \frac{1}{4}$ second on a 27-bit fractional part machine.

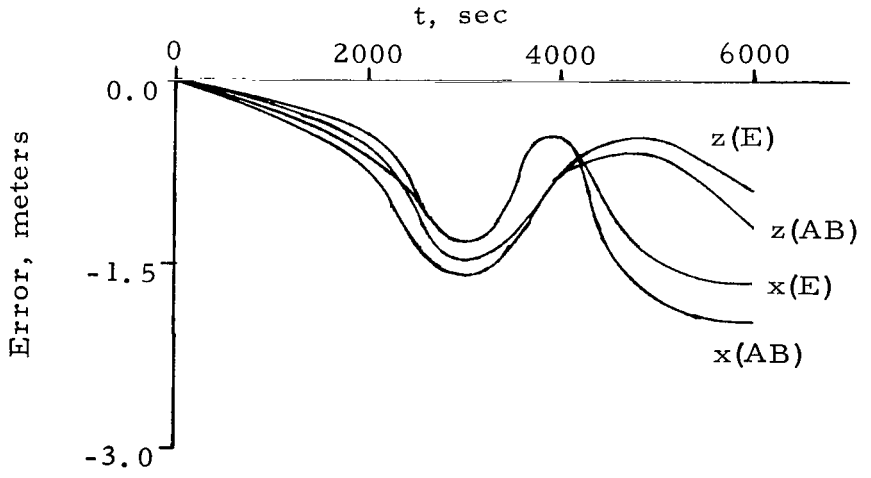


Figure 17.- Global error as function of time t in relative coordinates for $h = \frac{1}{32}$ second using Euler (E) and Adams-Bashforth (AB) second-order integration on a 27-bit fractional part machine.

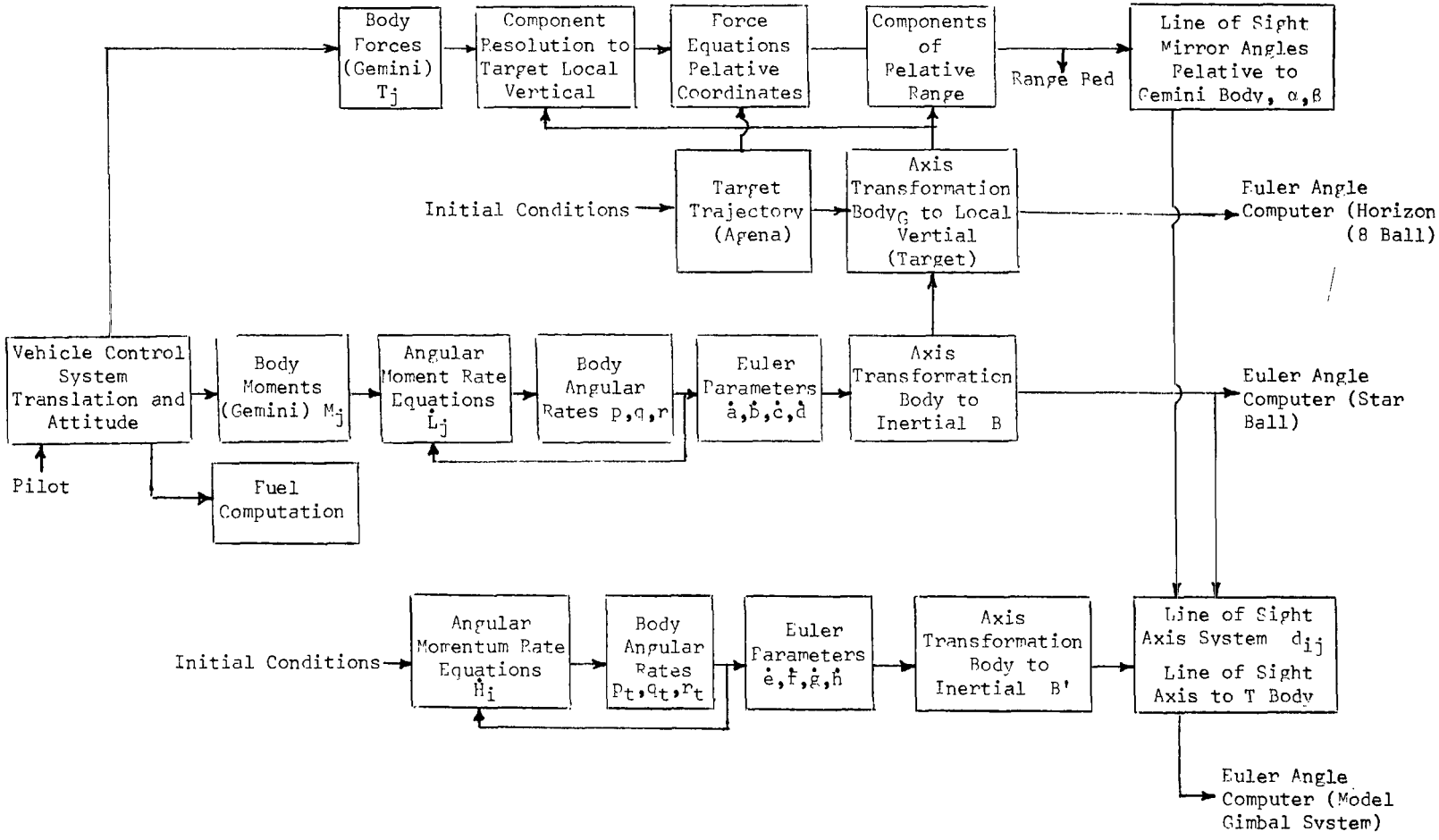


Figure 18.- Equation flow diagram.

*"The aeronautical and space activities of the United States shall be conducted so as to contribute . . . to the expansion of human knowledge of phenomena in the atmosphere and space. The Administration shall provide for the widest practicable and appropriate dissemination of information concerning its activities and the results thereof."*

—NATIONAL AERONAUTICS AND SPACE ACT OF 1958

# NASA SCIENTIFIC AND TECHNICAL PUBLICATIONS

TECHNICAL REPORTS: Scientific and technical information considered important, complete, and a lasting contribution to existing knowledge.

TECHNICAL NOTES: Information less broad in scope but nevertheless of importance as a contribution to existing knowledge.

TECHNICAL MEMORANDUMS: Information receiving limited distribution because of preliminary data, security classification, or other reasons.

CONTRACTOR REPORTS: Scientific and technical information generated under a NASA contract or grant and considered an important contribution to existing knowledge.

TECHNICAL TRANSLATIONS: Information published in a foreign language considered to merit NASA distribution in English.

SPECIAL PUBLICATIONS: Information derived from or of value to NASA activities. Publications include conference proceedings, monographs, data compilations, handbooks, sourcebooks, and special bibliographies.

TECHNOLOGY UTILIZATION PUBLICATIONS: Information on technology used by NASA that may be of particular interest in commercial and other non-aerospace applications. Publications include Tech Briefs, Technology Utilization Reports and Notes, and Technology Surveys.

*Details on the availability of these publications may be obtained from:*

**SCIENTIFIC AND TECHNICAL INFORMATION DIVISION**

**NATIONAL AERONAUTICS AND SPACE ADMINISTRATION**

**Washington, D.C. 20546**